Microwave Sensor Design for Non-Invasive Blood Glucose Measurement

Submitted to the Graduate School of Natural and Applied Sciences in partial fulfillment of the requirements for the degree of

Master of Science

in Electrical-Electronics Engineering

by

Mutahhar KURAN

ORCID 0000-0001-7992-8693

August, 2022

This is to certify that we have read the thesis **Microwave Sensor Design for Non-Invasive Blood Glucose Measurement** submitted by **Mutahhar KURAN**, and it has been judged to be successful, in scope and in quality, at the defense exam and accepted by our jury as a MASTER'S THESIS.

APPROVED BY:

Advisor: **Assoc. Prof. Dr. Merih Palandöken** ……………..
İzmir Kâtip Çelebi University

Committee Members:

Assoc. Prof. Dr. Merih Palandöken ……………..
İzmir Kâtip Çelebi University

Prof. Dr. Adnan Kaya ……………..
İzmir Kâtip Çelebi University

Assist. Prof. Dr. Şule Çolak ……………..
Eeeee University

Date of Defense: August 5, 2022

Declaration of Authorship

I, **Mutahhar KURAN**, declare that this thesis titled **Microwave Sensor Design for Non-Invasive Blood Glucose Measurement** and the work presented in it are my own. I confirm that:

- This work has been done wholly or mainly while in candidature for the Master's / Doctoral degree at this university.

- Where any part of this thesis has previously been submitted for a degree or any other qualification at this university or any other institution, this has been clearly stated.

- Where I have consulted the published work of others, this is always clearly attributed.

- Where I have quoted from the work of others, the source is always given. This thesis is entirely my own work, with the exception of such quotations.

- I have acknowledged all major sources of assistance.

- Where the thesis is based on work done by myself jointly with others, I have made clear exactly what has been done by others and what I have contributed myself.

Date: 05.08.2022

_____

Microwave Sensor Design for Non-Invasive Blood Glucose Measurement

Abstract

Diabetes management requires the use of detecting glucose content in blood. The detection of the glucose variation in characteristics of a tissue, RF approaches are promising to provide blood glucose measurements. This approach can provide a non-invasive observation of the amount of glucose in blood. The current research focuses on the development of a monitor that employs electromagnetic waves to non-invasively determine the amount of glucose in blood. A simulation model of fingertip together with a sensor element has been obtained to observe the impact of various glucose contents and responses of the sensor unit. The fingertip model is separated into four layers: blood, skin, fat, and bone. After the modelling of the multi-layer structure, the dielectric characteristics of each layer have been defined utilizing the Cole-Cole model parameters at 2.4 GHz. To investigate the capacity of the sensor element, two resonators are built that operate at microwave frequencies when put radiating towards human tissues. The initial prototype has been made from FR-4 material and had a 35 μm copper and a 1.6 mm dielectric substrate, by utilizing Eleven Lab PCB Prototyping Machine from Mits. Since the reflection coefficient of the first fabricated sensor element has not been matched with its simulation result, the optimized form of the sensor element has been fabricated. FR-4 material that has a permeability of 4.9 and a loss tangent of 0.024 has been utilized as the substrate. In order to perform in vitro tests, liquid phantoms that include sugar and water, have been prepared. The dielectric

characteristics of the phantom have been changed by varying the quantity of sugar. Liquid phantoms have been prepared, each containing distinct amount of sugar by weight. Finally, a measurement system has been constructed by combining the sensor element. For the measurement system, two XBee modules and the Arduino Uno board have been used. To get RSSI values to estimate glucose level in blood, the XBee modules have been configured to work as a receiver and transmitter. Once the wireless communication has been accomplished, a python code has been developed to detect variations in RSSI, which define variations of the glucose content in blood. The detection potential of variations in the resonance frequency of the sensor element has been enhanced by employing several machine learning techniques, to properly determine the amount of glucose in concentrations. Apart from the remarkable glucose level detecting capabilities for diabetes, the suggested RF sensing device has various additional advantages, including compact size, easy manufacture, cost, and minimum health danger.

Non-İnvaziv Kan Şekeri Ölçümü için Mikrodalga Sensör Tasarımı

Öz

Diyabet izleme, kan şekeri monitörlerinin kullanılmasını gerektirir. Biyolojik dokunun dielektrik özelliklerinde glikoza bağlı değişimi algılayarak, RF yaklaşımlarının kan şekeri ölçümlerini sağlaması umut vericidir. Bu yaklaşım non-invaziv ve sürekli kan şekeri takibi sağlayabilir. Mevcut araştırmalar, kan şekeri monitörlerini invaziv olmayan bir şekilde ölçmek için elektromanyetik dalgalar kullanan bir monitörün geliştirilmesine odaklanmaktadır. Yöntem, bir izleme cihazının rezonans frekansını, glikoz seviyesi ile ilgili olan kanın geçirgenliği ve iletkenliği ile ilişkilendirir. Değişen glikoz seviyelerinin etkisini ve sensör ünitesinin tepkisini incelemek için bir sensör ünitesi ile birlikte bir parmak ucu simülasyon modeli elde edilmiştir. Parmak ucu modeli dört katmana ayrılmıştır: deri, yağ, kan ve kemik. Çok katmanlı yapının modellenmesinden sonra, 2.4 GHz'de tek kutuplu Cole-Cole model parametreleri kullanılarak her katmanın dielektrik özellikleri tanımlanmıştır. Sensör ünitesinin performansını incelemek için mikrodalga frekanslarında çalışan iki rezonatör tasarlanmıştır. İlk prototip, Mits'den Eleven Lab PCB Prototipleme Makinesi kullanılarak basılmıştır. İlk imal edilen sensör elemanının yansıma katsayısı simülasyon sonucuyla eşleşmediğinden, sensör elemanının optimize edilmiş şekli imal edilmiştir. Bu sensör ünitesinin boyutu 42 mm x 80 mm x 1.6525 mm'dir. Substrat olarak 35 μm bakır kalınlığına ve 1.635 mm kalınlığında, geçirgenliği 4.9 olan FR-4 malzemesi kullanılmıştır. İn vitro testler yapmak için şeker ve su içeren sıvı fantomlar

hazırlandı. Fantomun dielektrik özellikleri, şeker miktarı değiştirilerek oluşturuldu. Son olarak, sensör ünitesinin bir ölçüm sistemi ile birleştirilmesiyle oluşturulmuştur. Ölçüm sistemi için iki XBee modülü ve Arduino Uno kartı kullanıldı. Kandaki glikoz seviyesini tahmin etmek için RSSI değerlerini elde etmek için, XBee modülleri bir alıcı ve verici olarak işlev görecek şekilde yapılandırıldı. XBee Explorer USB kartına monte edilen XBee modülleri, bir veri paketini sürekli yayınlayacak şekilde yapılandırıldı; böylece, Arduino'ya monte edilen alıcı XBee modülü düzenli RSSI değeri güncellemeleri alabilir. Kablosuz iletişim tamamlandıktan sonra, kan şekeri konsantrasyonundaki varyasyonları tanımlayan RSSI varyasyonlarını tespit etmek için bir python kodu oluşturulmuştur. Sensör elemanının frekans tepkilerindeki varyasyonların tespit potansiyeli, çeşitli konsantrasyonlardaki glikoz örneklerini doğru bir şekilde tespit etmek için çeşitli makine öğrenme teknikleri ölçüm düzeneğine dahil edilmiştir. Diyabet hastaları için dikkate değer glikoz seviyesi saptama yeteneklerinin yanı sıra, önerilen RF algılama cihazı, kompakt boyut, kolay üretim, maliyet ve minimum sağlık tehlikesi gibi çeşitli ek avantajlara sahiptir.

Anahtar Kelimeler: Diyabet, mikrodalga, glukoz sensörü, makine öğrenmesi

To my grandfather…

Acknowledgment

Many thanks to my my supervisor Assoc. Prof. Dr. Merih PALANDÖKEN for his guidance, trust, and time that I received during this thesis.

I would also like to thank Research Assistant Caner Murat, Research Assistant İsmail Akdağ, and Research Assistant Cem Göçen for their support and friendship.

I especially express my deepest gratitude to my family and friends for their support and encouragement.

Table of Contents

List of Figures

List of Tables

List of Abbreviations

AC	Alternating Current
DC	Direct Current
PCB	Printed Circuit Board
EM	Electromagnetic
RF	Radio Frequency
FR4	Fiberglass Reinforced Epoxy
3D	Three-Dimensional
CST	CST Microwave Studio
NHS	National Health Service
WHO	World Health Organization
SMBG	Self-Monitoring Blood Glucose
CMG	Continuous Monitoring Glucose
FDA	Food and Drug Administration
ISF	Interstitial Fluid
BGL	Blood Glucose Level
NIR	Near-infrared spectroscopy
MIIR	Mid-infrared spectroscopy
OCT	Optical Coherence Tomography
IS	Impedance Spectroscopy
VNA	Vector Network Anlayzer
DUT	Device Under Test
MCU	Micro Controller Unit

UART	Universal Asynchronous Receiver-Transmitter
SIW	Substrate Integrated Waveguide
SRR	Split-Ring Resonator
CSRR	Complementary Split-Ring Resonator
MUT	Material Under Test
BGM	Blood Glucose Monitoring
MICS	Medical Implant Communication Service
ISM Band	Industrial, Scientific and Medical Radio Band
MSL	Microstrip Line
CPW	Coplanar Waveguide
GCPW	Coplanar Waveguide with the Ground Plane
HCFA	Hilbert Curve Fractal Antenna
DAK	Dielectric Assessment Kit
RSSI	Received Signal Strength Indicator
SVR	Support Vector Regressor
DTR	Decision Tree Regressor
PR	Polynomial Regressor
RFR	Random Forest Regressor
BR	Bagging Regressor
ABR	Ada Boost Regressor
GBR	Gradient Boosting Regressor
LGBR	Gradient Boosting Regressor
CBR	Cat Boost Regressor
MSE	Mean Square Error
MAE	Mean Absolute Error
RMSE	Root Mean Squared Error

List of Symbols

λ	Wavelength
ε_r	Dielectric constant
Ω	Electrical unit of resistance
ε_{eff}	Effective dielectric constant
f_C	Center frequency
ε'	Real dielectric constant
ε''	Imaginary dielectric constant
σ_e	Effective conductivity
Q	Quality factor
$\vec{D}$	Electric flux density
$\vec{B}$	Magnetic flux density
f_r	Resonance frequency
L_{eff}	Effective length of a resonator
ε_{eff}	Effective dielectric constant
c	Speed of light

Chapter 1

Introduction

1.1 Diabetes

Diabetes is a common metabolic illness that appears without any apparent reason and is caused by the breakdown of the glucose control system represented in Figure 1.1.
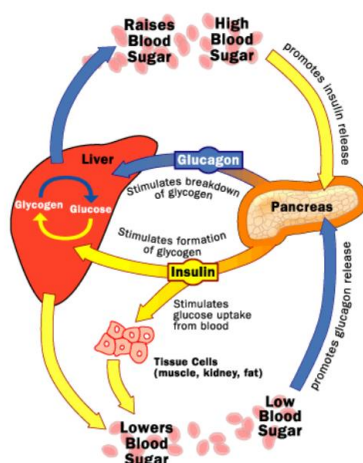
Figure 1.1: The mechanism of glucose regulation in the body [2]

It can be caused heart disease, renal disease, strokes, eyesight loss, amputation, and difficulties in the neurological system, [6,7]. Therefore, keeping a normal BGL is critical in our lives.

1.2 Glucose Monitoring Techniques

Clinical research has shown that people with diabetes who take insulin or do not use insulin benefit from self-detecting of BGLs [6]. The traditional SMBG technique,

which involves drawing samples of blood from the finger prick methodology, or CMG can be used to check a people's BGLs [3]. Since it may be necessary for patients to evaluate their BGL at least eight to ten times every per a day, this repetitive technique of finger pricking may be uncomfortable [10] and, over time, lead to calluses [11]. Furthermore, for persons who assess their BGLs numerous times each day, the measurement strips might add up to be a substantial expense [11]. So, it is critical to develop a simple, non-invasive, low-cost, continuous, and user-friendly glucometer. Non-invasive methods might eliminate the utilization of an implant, finger pricking, and disposable needle-like electrodes. However, external factors such as sweat, body temperature, skin hydration, diffrences in the surface of skin, and physical movement poses a difficulty for non-invasive glucose detecting systems [10].

Over the last few decades, non-invasive glucose monitoring systems have received considerable attention. Breath Chemical Analysis, ISF Analysis, Infrared Spectroscopy, Temperature Modulated Localized Reflectance, OCT, Raman Spectroscopy, Ultrasound, Polarity Changes, Fluorescence, Thermal Spectroscopy, IS, Ocular Spectroscopy and RF Spectroscopy are the different types of spectroscopies. ISF analysis is the most like conventional monitoring of all non-invasive monitoring methods. There is an enzymatic process that utilizes ISF on skin. Glucowatch, created by Cygnus [4], was the most prominent ISF glucose monitor. The monitor was in the shape of a watch, and the ISF has been absorbed by a replaceable pad pressed against the skin. In multiple clinical trials [5, 6], the Glucowatch has been proved to accurately detect blood glucose levels and has been certified by the FDA in 2001. However, the firm has been shut down in 2005. It has been claimed that this was due to technical problems and high user expenses [7]. It is unclear whether comparable strategies are being employed for new products now. The detection of acetone in exhaled breath is a different type of chemical analysis approach. A method that can chemically analyze exhaled air and calculate blood glucose levels has been developed [8]. NIR and MIIR are the two types of infrared spectroscopy. NIR is a lower frequency technique that uses infrared light transmission and reflection to measure blood glucose levels [9]. NIR may be used in four different evaluation types: transmission, diffuse reflectance, transfectants, and photoacoustic [10]. MIIR employs almost the same approach as NIR, except there is often insufficient light penetration at MIIR frequencies to perform transmission analysis. As a consequence, reflection analysis is the main method

employed. Infrared spectroscopy has not yet to been demonstrated as a valid measuring tool. OCT utlizes the measurement of light scattering. Another type of light scattering measurement is temperature-modulated localized reflectance. The refractive index of the tissue varies with temperature, but the change is also affected by glucose contents [11]. Raman spectroscopy is a technique that generates a fluid oscillation, causing variations in characteristics of light scattering [12]. The possibility of interference from other molecules is a disadvantage of this approach. The change in polarization is also an optical approach that has been studied in the eye. While this approach is practicable, great specificity has indeed been hampered by pH and interfering chemicals. There is a potential technology for detecting glucose content that makes use of ultrasound. A short laser burst has been utilized to burn a tiny region of tissue. The frequency of the laser determines the photoacoustic excitation. The photoacoustic spectrum may be used to detect the concentration of glucose in fluids when the laser frequency is changed [13]. The research shown that fluorescence may be used to predict glucose concentrations [9]. This has demonstrated great potential because the intensity is heavily influenced by skin pigmentation and thickness. The examination of infrared radiation emitted by the human body is known as thermal spectroscopy. While some other parameters are important, glucose content is proven to have an absorbent influence on the infrared emission produced by the human body [4]. Ocular spectroscopy is a way of chemically analyzing tears to determine glucose levels. A contact lens that responds with the glucose in tears has been developed [14]. When light is emitted from a source of light, the wavelength of the light reflected varies depending on the glucose content, which may be detected with a spectrometer. Another well-studied technology is IS, which examines changes the characteristics of blood in a non-invasive manner. BGL variation influences the electrical characteristics of erythrocyte membranes [15, 16]. The IS approach can identify these fluctuations by calculating impedance magnitude, |Z| by utilizing a RLC resonant circuit [17] or a VNA. The chemical structure of materials influences how microwave interacts with them. Thus, specific tissue and fluid compositions may be determined by monitoring the reaction of the molecules following stimulation. These electromagnetic waves may penetrate human tissue and biocompatible materials to varying degrees depending on the frequency (wavelength), enabling non-invasive, individually targeted monitoring. Changes in the electromagnetic wave propagation in a liquid medium biomaterial are

translated into a measurable signal by microwave biosensors. The transducer, on the other hand, is unable of identifying whether the variation in permittivity is because of the protein variation or the change of glucose content in blood. As a result, models that characterize a material's permittivity throughout a frequency range are necessary.

Over the last two decades, various works have gone into developing non-invasive glucose monitoring systems. Nonetheless, non-invasive solutions mostly failed to reach the required accuracy standards and couldn't run for an extended length of time. To model the relation between BGL and the characteristics of blood, the equation of Cole-Cole has been utilized in [18]. To investigate blood glucose dependence, several blood samples have been taken and modified in vitro. According to the findings of the research, non-invasive devices require more research to account for the effects of other biological tissues such as fat, muscle, and skin. Another test has been carried out to see if there was a link between changes in microwaves resonance characteristics and changes in BGL [2]. Two different blood samles have been located into a test cell and subjected to EM energy from 10 to 20 GHz with low power. The system's S_{21} magnitude response has been determined with a VNA for both cases, as illustrated in Fig. 1.2. The frequency change has obseerved by a change in the permittivity of the BGLs. Furthermore, the first sample's Q factor was larger than the second samples. Both investigations demonstrated that microwave monitoring is a potential method for non-invasively detecting BGLs. Nevertheless, in-vivo electrical characteristic measurements, as well as the influence of other factors in blood on electrical characteristics, should always be researched further.
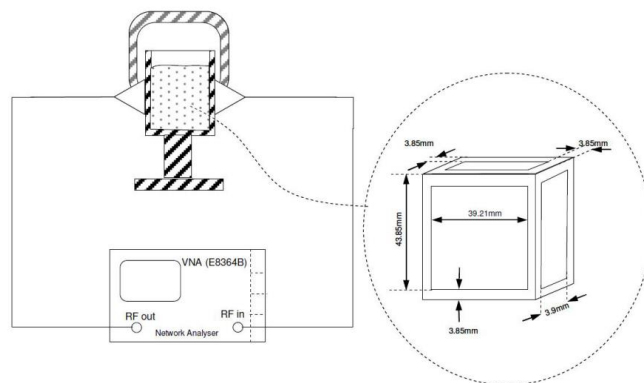
Figure 1.2: The setup for the measurements of test cells in between the antennas [2]

The ε'and ε" of blood increase when glucose content in a sample drop, according to a study done in [19]. The glucose dependency illustrated in Figure 1.3 is the outcome of the data obtained.
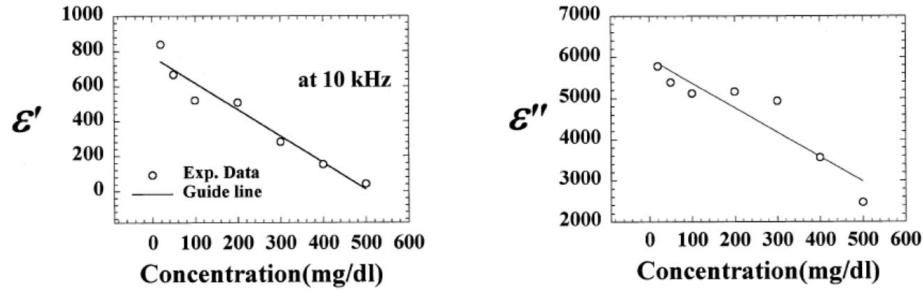
Figure 1.3: The dielectric constant dependent on water/glucose concentration [19]

The ε_r and σ of blood and fluids fluctuate through changes in BGLs, as previously described. Nevertheless, only a few comprehensive studies have been published that analyze variations permittivity and effective conductivity as a function of BGL. With the insertion of liquid D-glucose to blood plasma collected from people, Topsakal et al. [20] measured dielectric properties. For each measurement, the amount of dextrose in the blood has been increased. At room temperature, readings have been done by administering liquid dextrose. The trials have been carried out with an open-ended thin probe, which may measure frequencies between 500 MHz and 20 GHz.

Despite the fact that the test has been conducted on a tiny sample, the findings shed light on the link between BGL and dielectric characteristics. Figures 1.4 depicts the ε_r and σ of a blood sample that has various dextrose concentrations. Blood plasma's relative permittivity and effective conductivity both decreased when glucose levels increased. It's worth noting that typical BGL is 80 mg/dl when fasting and 140 mg/dl after eating. The ability to construct a sensitive microwave device requires a realistic glucose dependence of dielectric characteristics. The ability to develop a microwave device which is sensitive to detect variations requires a realistic glucose dependence of dielectric characteristics.

<p style="text-align:center">(a)   (b)</p>
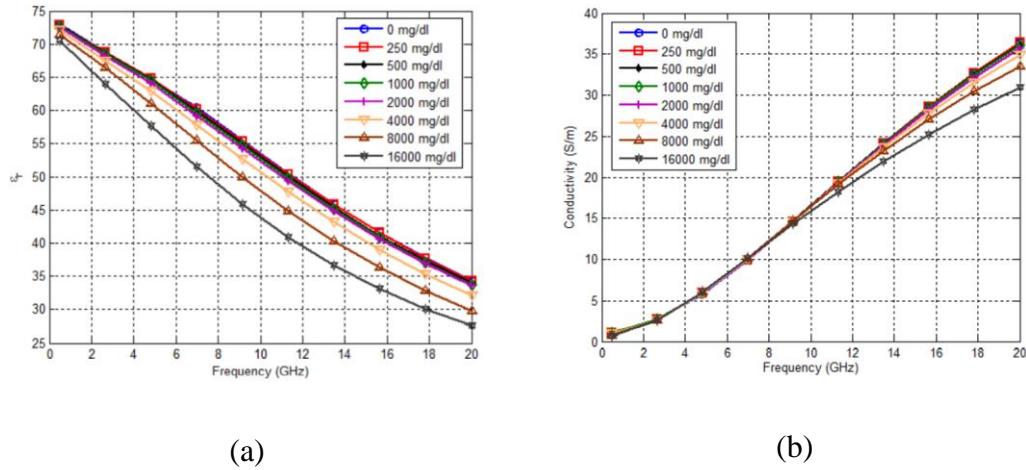
Figure 1.4: (a) Glucose levels concentration versus Blood plasma: (a) Relative permittivity and (b) Electrical conductivity [20]

Through the rapid technological developments of millimeter and microwave circuits in wireless system design [21, 22], versatile circuit design techniques have been employed in wireless component design including microwave filters. Microstrip filters have various applications covering radars, cellular communication, test, and measurement systems [33]. It is due to the ability of designing unique microwave components with smaller sizes and higher performance through the introduction of novel artificial materials [23]–26]. A microwave filter is one component of a communication system that frequently requires modification. It is due to the growing need for high performance in a small package with low insertion loss, good selectivity, and low cost [27]. A microwave filter is a type of two-output circuit. This circuit is used to detect the frequency change [33]. In parallel with the developing technology, monitoring of various parameters related to the patient has become of great importance. Developments in these medical fields include diabetes, etc. it has significantly improved the quality of life of people who have to live with their ailments. With this system, which allows remote monitoring of the patient, intervention can be performed on the patient without has been-ting time [35]. In [28], a novel microwave sensor design has been introduced for not only the dielectric parameter characterization of water-ethanol mixtures having different ethanol concentrations but also the volumetric concentration determination of ethanol in the liquid mixture. In [29], a metamaterial based CSRR have been presented as a microwave sensing device for the characterization of a liquid, as shown in Figure 1.5.

By utilizing CST simulation software, two sensor configurations have been created, tested, and verified, as shown in Figure 1.6. The advantages of the proposed sensors allow for multiple quick and simple measurements to be made using various test tubes, which speeds up, simplifies, and reduces the cost.
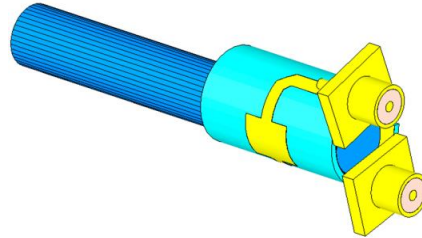
Figure 1.5: The implemented sensor with embedded glass tube [29]
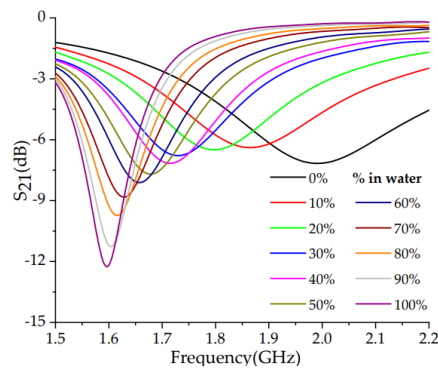
Figure 1.6: The simulation results of proposed sensor for S_{21} parameter [29]

[30] presents a portable and non-invasive sensing structure for detecting BGL of a subject. The tongue has been chosen a since it is a highly stable location with no significant alterations. Furthermore, the high blood-tissue ratio ensures a significant presence of blood in the measurement region. The tongue's temperature stability is also the desired quality. A low-cost scalar network analyser served as the sensor controlling electronics. Figure 1.7 depicts the concept and the implemented scalar network analyser.
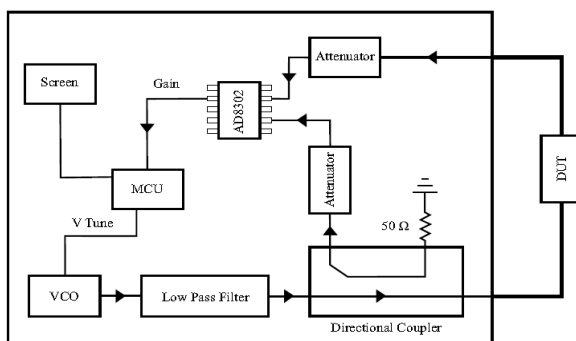
Figure 1.7: The schematic of the scalar network analyser [30]

After detection, the magnitude S_{21} parameter, or DUT transmission signal, is acquired. A tactile screen with a user interface has been also included, which has been coupled to the MCU through UART. The screen enabled users to enter specific data and do measurements, as well as view the resulting graph. Figure 1.8 shows an image of a person taking a measurement. After the gadgets have been built, they have been tested in the lab with several volunteers to see how well they worked. The volunteers took a test with the gadget at the start of the experiment (after an 8-hour fast), then drank a sugared drink, and thereafter took repeated measures every few minutes. The findings do not demonstrate a complete match between the measured magnitude and the goal magnitude, according to the raw data.
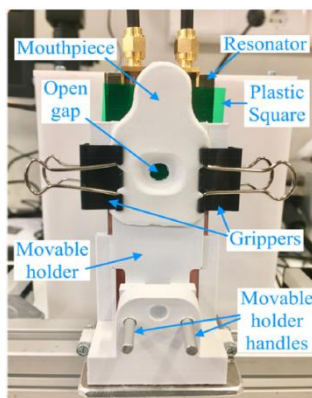
Figure 1.8: The sensor setup [30]

For realizing a configuration for BGL detection, a band-stop filter in SIW is recommended in [31], as shown in Figure 1.9.
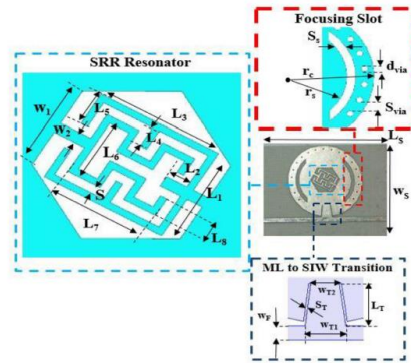
Figure 1.9: The suggested sensor architecture [31]

The suggested SRR may significantly boost the electric field density in certain places around the sensing zone. The suggested SRR's equivalent circuit model is shown in Figure 1.10. Since the curved slots has a substantial impact, the EM distribution of the suggested sensor is more concentrated in the center of the SIW, as you can see from in Figure 1.11.
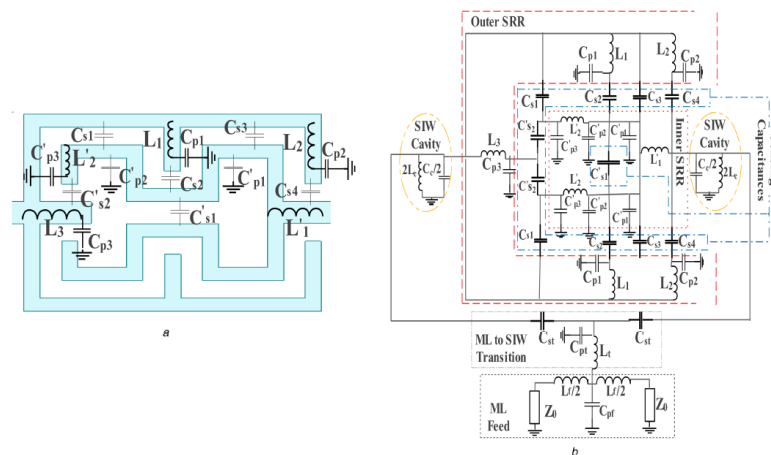
Figure 1.10: The proposed SRR and its equivalent circuit model [31]
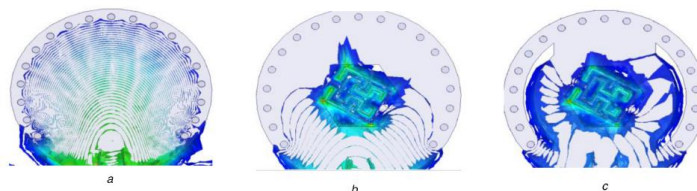
Figure 1.11: The impact of sensor elements on the distribution of electric fields [31]

A measuring strategy is offered for calculating the uncertainties of the suggested sensor performance. It contains: the BGLs of patients are measured using a

GLUCOCARDTM 01-mini, and the detection of BGLs is also conducted by pressing their fingers on the sensing region of the sensor. The observed findings of the sensor are shown in Figure 1.12. For BGL monitoring, the sensor has a high sampling error of roughly 32%.
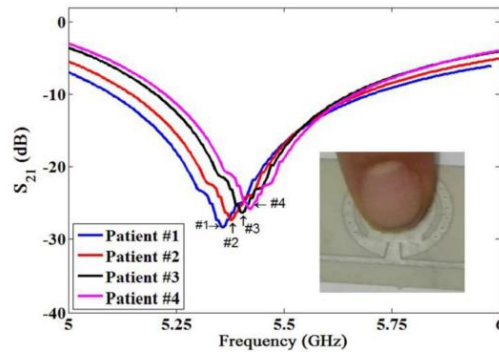
Figure 1.12: The suggested sensor's measured findings [31]

[32] proposes a one-port microwave resonator that is depicted in Figure 1.13. The sensor's Q-factor has been found to be smaller in the tested case, allowing resonance in wideband.
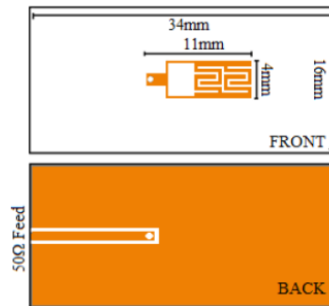
Figure 1.13: Layout of the designed sensor [32]

For a reproducible reading, it's important to remember that the fingertip needs to cover the detecting surface and be located in the accurate place all time. Alternatively, various amounts of fringing fields with uncertain fractions may occur in air and tissue layers, resulting a change in the response of the sensor. So, putting the sensor in a shell that can fit a finger, the position may be readily adjusted. As seen in Figure 1.14, such a shell has been customized and utilized.
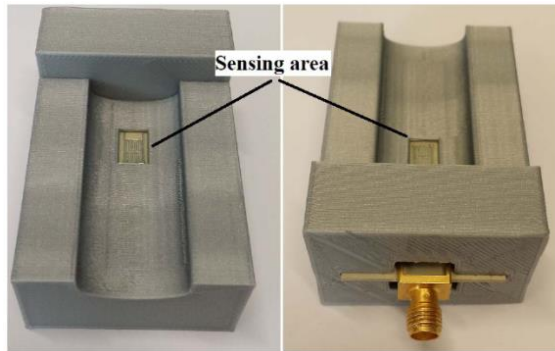
Figure 1.14: 3D printed sensor case [32]

The tests also revealed that a fingertip reading is particularly sensitive to the amount of pressure being applied. Two innovative pressure sensor circuits have been presented to overcome this problem. The suggested circuits' circuit block diagrams are illustrated in Figure 1.15. Figure 1.16 shows photos of the intended and implemented circuits.
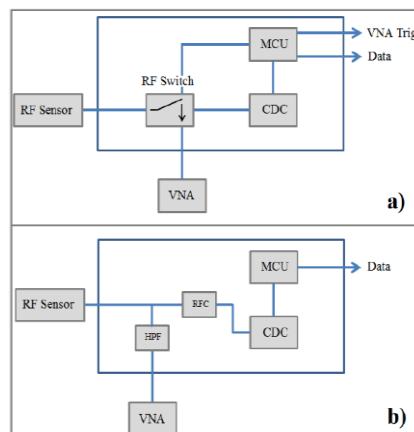
Figure 1.15: Circuit diagrams for the versions: (a) 1, and (b) 2 [39]
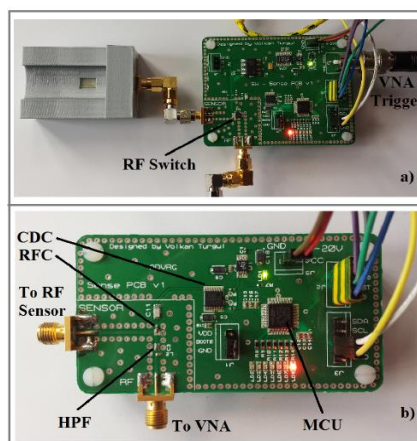
Figure 1.16: Circuit photographs of the versions: (a) 1, and (b) 2 [32]

A microwave detector with a J-shape has been utilized in [33] to measure BGLs. Rectangular patches with four J-shape constructions have been placed on the four edges to illustrate the resonator's connected and unconnected states. Figure 1.17 depicts the sensor model.

(a)   (b)
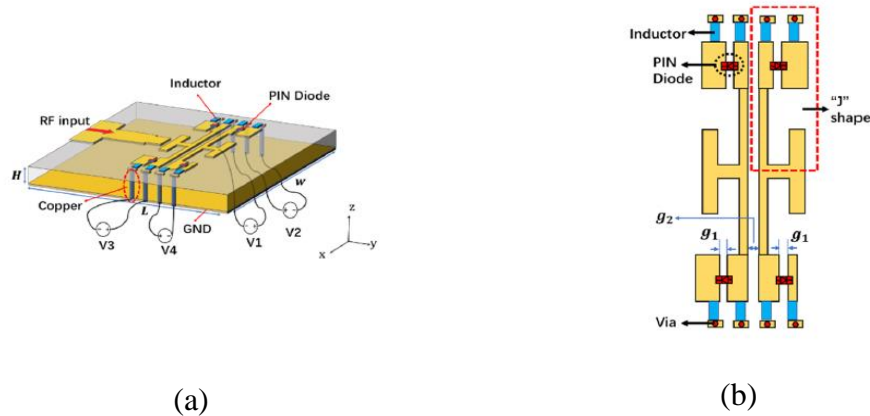
Figure 1.17: (a) 3D illustration of the suggested model, (b) Four-J-shape patch [33]

To boost the efficiency rate, the authors use PIN diodes instead of rectangular patches. The six uniformly distributed simulated states and the simulation of frequency change without PIN diode for two distinct values of ε_r are given in Figure 1.18. It may be stated that f and S_{11} have improved dramatically after the addition of PIN diodes.

(a)   (b)
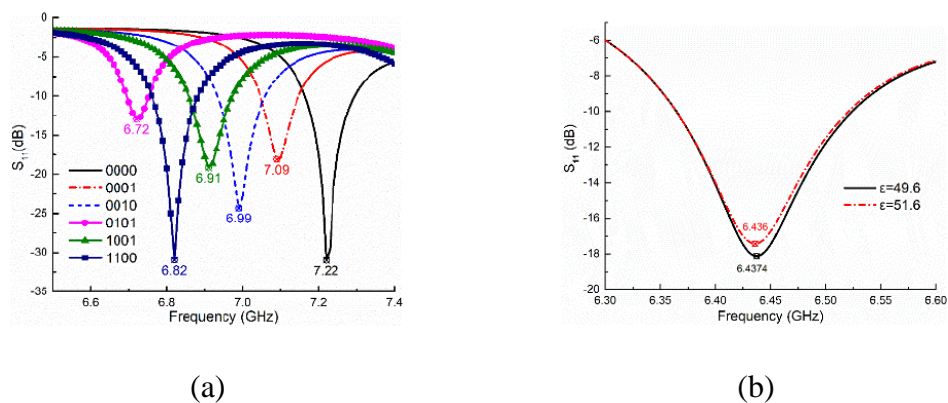
Figure 1.18: (a) The six uniformly distributed simulated states; (b) The shift in frequency without PIN diode at ε_r =49.6 and 51.6 [33]

In [34], a bandpass filter that works as a glucometer has been presented. Once this design is connected to the patient's thumb, the permittivity of the thumb, as a

superstrate, changes depending on the patient's BGL, and thus the filter's response is modified. The BGL may be precisely estimated by using this fluctuation and its normalization. Even though the substrate's permittivity is stable, the finger functions as a superstrate and variations in BGL produce a change in the bandpass filter's resonant frequency. Figure 1.19 depicts the suggested patch configuration, which consists of a patch, a slot, a ground plane, and a substrate.
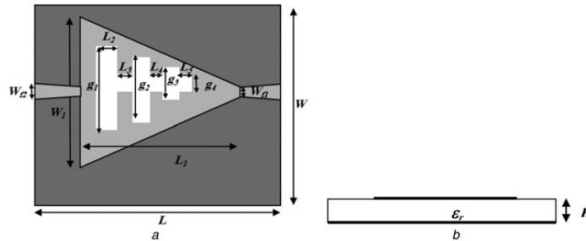
Figure 1.19: The structure of filter [34]

To test the functionality, an individual lays his thumb on the filter 4 hours after a typical breakfast. The HP8720ES VNA has been used to evaluate the filter's response. Figure 1.20 depicts the test and simulation findings for this case.

(a)

(b)
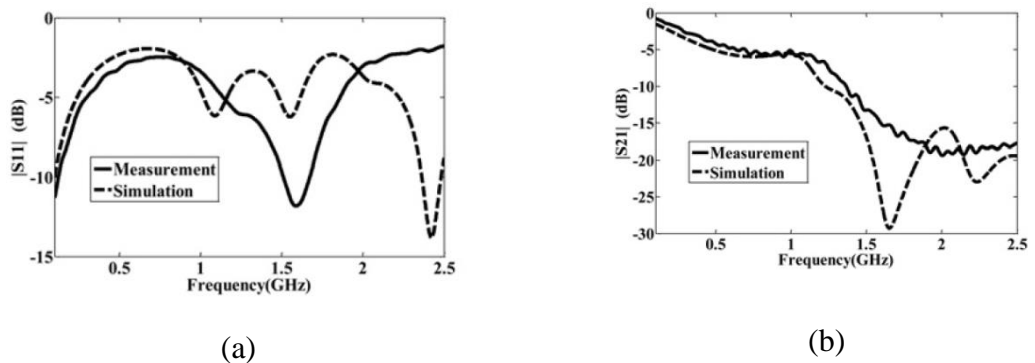
Figure 1.20: Simulation and measurement results of the filter with a thumb on top of the filter (a) $|S_{11}|$; (b) $|S_{21}|$ [34]

As the figures show, there are a few variations between simulation and experimental outcomes. Following that, the individual uses sugary water with high glucose concentration, and the test is done four times more. Figure Figure 1.21 depicts the results of these tests. Based on these findings, it is obvious that the sensors are able to monitor linear glucose content variations in blood.
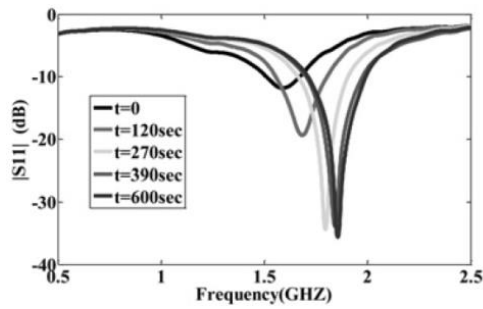
(a)
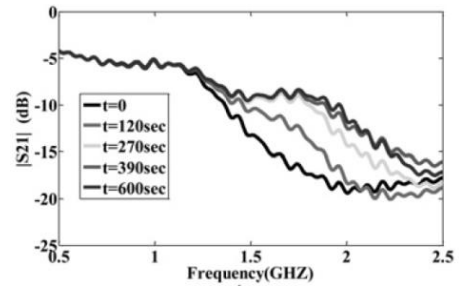
(b)

Figure 1.21: Simulation versus measurement results of the filter with a thumb on top of the filter after the sugar water (a) |S11|; (b) |S21| [34]

As seen in Figure 1.22, the microstrip ring-resonator has been designed to develop the sensing architecture for BGL detection [35] Simultaneously, a commercialized glucometer has been utilized to detect BGLs. The change in S_{21}'s initial maximum has been monitored. The design is meant to work in the MICS band; nevertheless, it operates at 465 MHz when attached to a human wrist. The initial max of the S_{21} has been enhanced by 8.5 MHz during the soda test. Nevertheless, the operator didn't reveal a correlation between glucose levels and max shift. In addition, no pressure has been applied during the test. It is well accepted that pressure has a considerable impact on the resonance response.
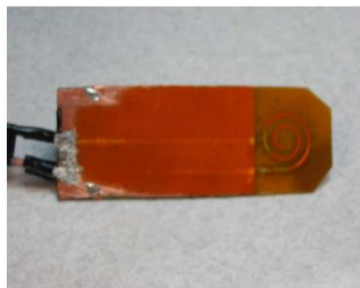
(a)

(b)

Figure 1.22: (a) The first design of suggested sensor (b) with silicon positioning case [35]

As illustrated in Figure 1.23, the time sensor has been adapted to capture readings through the thumb. With off-the-shelf monitoring equipment, 5 participants have been asked to monitor the capillary BGL. The volunteers have been then instructed to apply regulated pressure to the resonator using their thumb. The resonator's reaction is then recorded. The sensor is calibrated using the data acquired from the participants. Nonetheless, the operator didn't provide any technique specifics, and no definition of the mistake has been provided. The calibration outcomes have been provided, but the technology hasn't been clinically tested.
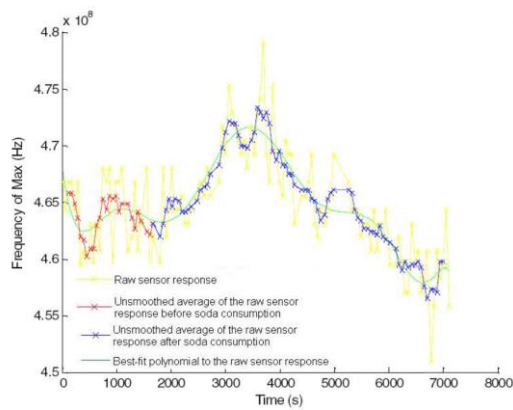
Figure 1.23: The variation in the initial maximum of S_{21} [35]

Since it has a good supply of blood, the fingertip is the most popular place to take a sample of blood for traditional procedures, and an ideal measuring place for non-invasive microwave BGL studies. Moreover, positioning the fingertip on the sensor is simple. Also, a positional mistake may induce a greater frequency change than the change because of the variations in BGL. [36] studied any influence of fingertip placement on the sensor. To show this, simulations have been run using both the standard 4-layer fingertip simulation model and a unique model having a fingerprint imprinted on it. The four-layer fingertip model has been created in CST MWS using fat, skin, bone, and blood layers with the dielectric constant and thickness values presented in Figure 1.24.
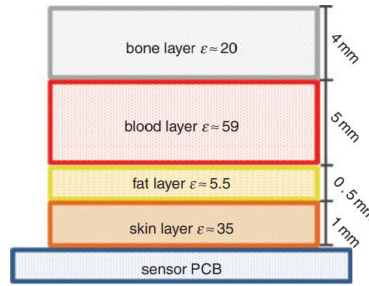
Figure 1.24: The 4-layer fingertip model [36]

The sensor has been examined using glucose/water mixtures as a mimic for glucose content. Nonetheless, due to abnormalities, the projected shift was significantly smaller than expected. The obtained operating frequency values have been then normalized to the operating frequency in MATLAB. The operating frequency is affected by the location of the fingertip on the sensor, as shown in Figure 1.25, with the amount of the influence depending on the position. Due to the asymmetric structure of the fingerprint, the change generated in any of the quadrants of the graph is not uniform regarding the origin. This error might lead to completely incorrect readings. As a result, special consideration should be given to the placement of the fingertip on the sensor, where the irregularities of the fingerprint increase the amount of failure.
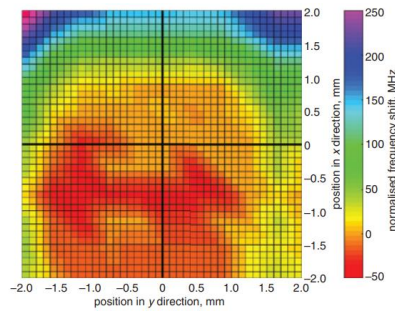
Figure 1.25: Normalized frequency change in relation to sensor fingertip location
[36]

A novel voxelized blood model [37] has been examined and suggested. Figure 1.26 shows an original and a voxelized models in CST. While a voxel-based technique may provide great three-dimensional geometric representations of the thumb, it is impossible to account for the complicated permittivity of blood and glucose content in a voxel model.
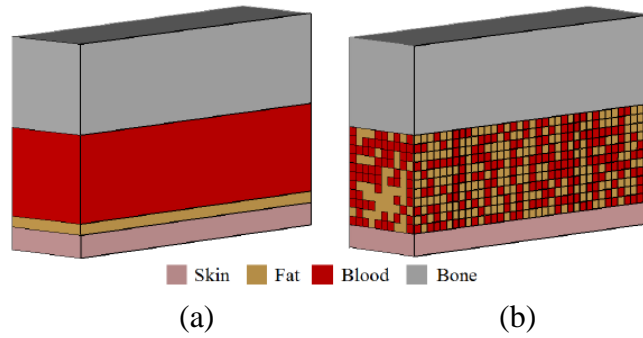
Figure 1.26: The 4-layer fingertip illustrations: (a) original (b) voxelized [37]

In [38], the blood has been characterized as a "Cole-Cole material" to measure the ε_r dependency as a function of glucose in blood. CST been utilized to create a 3D thumb model, as shown in Figure 1.27.
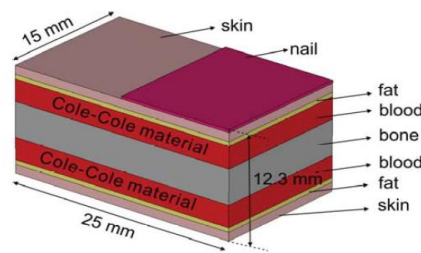
Figure 1.27: 3D EM model of thumb in CST MWS [38]

[1] describes the schematic of a thumb model which has four layers, as illustrated in Figure 1.28. The blood permittivity of the thumb model has been altered from hypoglycemia to hyperglycemia levels to test the suggested sensors, resulting in ε_r values of 55–65.
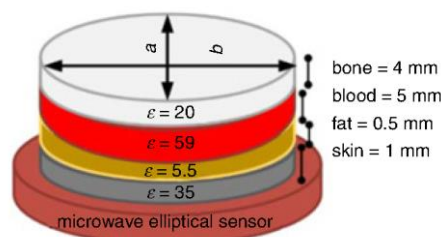
Figure 1.28: The 4-layer thumb model located on the RF sensor [1]

To mimic the biological tissue, a four-layered digital phantom has been constructed and put just above the resonator as a superstrate in [2], as shown in Figure 1.29.
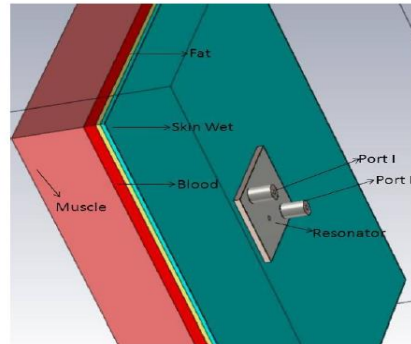
Figure 1.29: The 4-layered digital phantom placed on top of the resonator [2]

In [39], CST MWS has been used to build a simple model of the body's various tissues, including the second-order Debye formula. This model is shown in Figure 1.30. To match the wideband dielectric characteristics at distinct BGLs, the equation of Cole-Cole has been utilized in [40].
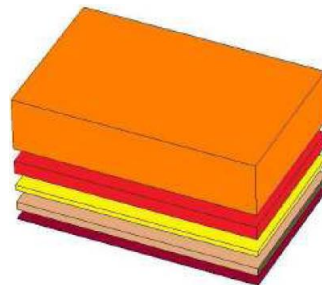
Figure 1.30: The layers of the finger model [39]

Utilizing ultrasound technology, a qualification of the little finger has been done in [41]. This has been done to calculate realistic layer thickness values. Ultrasound measurements have been used to identify the physical characteristics of each layer. It has been supposed that these layers have been homogenous. Figure 1.31 depicts a depiction of the layers and their properties. Following the modeling, the electromagnetic characteristics of the tissues have been described utilizing second-order Debye approximation and parameters from [42] for the range of 0.5-20 GHz.

Tissue	Thickness [mm]	ε'_∞	$\Delta\varepsilon'_1$	$\Delta\varepsilon'_2$	$\tau_1[10^{-12}S]$	$\tau_2[10^{-12}S]$
Dry Skin	0.6	4.39	32.87	65.8	7.42	574
Wet Skin	1.04	6.04	37.6	74.9	7.52	734
U. Blood	0.1	6.68	53.6	406	7.84	2404
Bone	4	3.38	9.01	6.76	10.9	381
Muscle	2	6.47	47.7	186	6.79	1827
Blood	0.25	6.68	53.6	406	7.84	2404
Fat	2.3	3.39	8.08	16.7	6.91	1635
Blood						
Wet Skin						
Dry Skin						

Figure 1.31: The ultrasound model and the parameters for the little finger layers [41]

The developed microwave resonator, which dictates the strength of its contact with the material under test, was a significant issue. Then, the finger becomes a component of the sensor. The electromagnetic field distribution has been studied for different types of planar constructions: CPW, MSL, and GCPW. A band-stop filter with three connected lines has been chosen as the microstrip line structure. After that, a CPW topology has been generated using a similar method. To begin, a single, straight conducting line with an arbitrary width has been utilized. After then, the GCPW has been created. The f_R of the scattering parameters of the three simulated topologies is shown in Figure 1.32. The picture also depicts how each curve responds to changes in the ε_r of blood. In simulations, the ε_1 parameter's range of variation was considerable. This has been done to allow for substantial-frequency changes when comparing the planar structures. It could help confirm the sensors' performance across a wide frequency spectrum. It's also worth noting that the Q changes due to the conditions. The ε'' impacted ε_1, is responsible for this phenomenon.
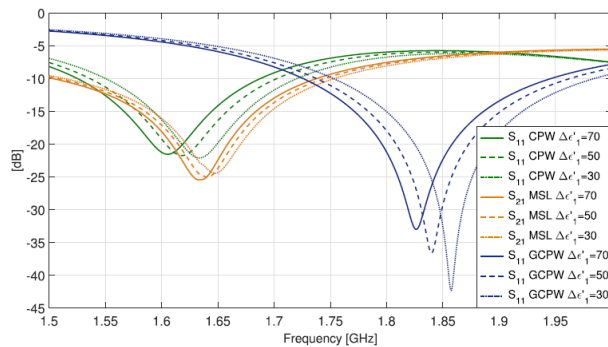
Figure 1.32: Comparison of topologies under consideration due to variations of glucose content in blood [41]

To secure the sample and reduce any errors in each measurement because of its location, a white plastic container has been customized to fit the little finger of a subject. Figure 1.33 depicts a sample that has been developed.

Figure 1.33: The implemented GCPW sensor prototype [41]

Figure 1.34 depicts the progression of the test. As can be observed, the finger-sensor system's resonance frequency developed in a very comparable manner to BGLs.
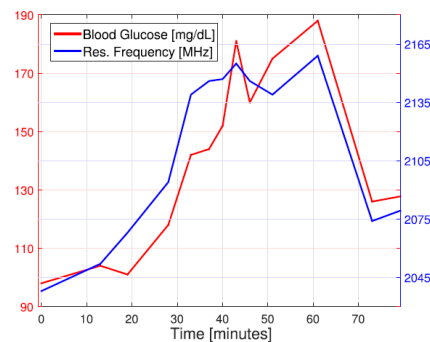
Figure 1.34: Operating frequency and measured BGLs versus time [41]

1.3 Research Objective

The thesis aims the development of the non-invasive and microwave blood glucose monitoring device. The research objectives are:

1. To explore the relationship between the blood glucose level and dielectric properties of biological tissue,

2. Numerical model design for the sensor element and a fingertip,

3. Numerical investigation of the response of the sensor element with respect to the variations in blood glucose level,

4. Experimental analysis of the sensor element prototypes,

5. Establishing the relation between the resonance frequency of the sensor element and glucose concentration using tissue mimicking phantoms,

6. Development of the measurement system,

7. Blood glucose level estimations via Machine Learning Algorithms.

1.4   Thesis Organization

The thesis is sectioned into six chapters.

Chapter 1 presents a review of glucose detecting, followed by a overview of current authorized self-detecting glucose systems and related limitations, as well as the reason for this study as an alternative for a self-detecting the amount of glucose in blood. This chapter also includes the research aim and thesis structure.

Chapter 2 will address the theoretical background and the properties of blood. Additionally, the chapter gives an overview of the background knowledge required to create a glucose dependent model.

Chapter 3 focuses on numerically modeling the non-invasive microwave sensor element and fingertip. Furthermore, this chapter includes numerical analyses that examine the reaction of the senor element to changes in BGL.

Chapter 4 will give a prototype of a non-invasive sensor element and in vitro tests that observe the effect of the BGL to the response of the senor element.

Chapter 5 presents the development of the measurement system to automatically compute the variations in BGL. The collected data will also be analyzed.

Finally, Chapter 6 summarizes this research conducted throughout the thesis and discusses future work that might be done to improve the measuring method presented in this thesis.

Chapter 2

Background

2.1 Theory

Dielectric characteristics are parameters that describe how materials behave in the presence of an electric field. Maxwell's equations can be used to describe dielectric characteristics. If we assume that time-varying fields are in a medium, the Maxwell's equations can be stated as follows;

$$\overrightarrow{\nabla} \cdot \vec{D} = \rho_v \tag{2.1}$$

$$\vec{\nabla} \times \vec{E} = -\frac{\partial \vec{B}}{\partial t} \tag{2.2}$$

$$\overrightarrow{\nabla} \cdot \vec{B} = 0 \tag{2.3}$$

$$\vec{\nabla} \times \vec{H} = \vec{J}_c - \frac{\partial \vec{D}}{\partial t} \tag{2.4}$$

ρ_v stands for volume charge density, $\vec{J}_c$ stands for conduction current density, while $\vec{E}$ and $\vec{H}$ stand for electric and magnetic fields, respectively. The medium's constitutive properties, notably permittivity and conductivity, may be calculated using the field equations. In order to do this, equation 2.4 is expressed in phasor form. Equation 2.5 may also be obtained by inserting constitutive equations $\vec{D} = \varepsilon_0 \varepsilon_r \vec{E}$ and $\vec{J}_c = \sigma \vec{E}$.

$$\vec{\nabla} \times \vec{H} = \sigma \vec{E} + j\omega\varepsilon_0\varepsilon_r\vec{E} \tag{2.5}$$

Permittivity refers to a material's ability to retain energy, specifically its ability to align its molecules through the applied field. The material's conductivity indicates the loss. Conduction current represents power loss. Also, the spinning of the dipole molecules results in energy loss owing to friction. As a result, equation 2.5 should be revised to incorporate the additional source of loss, $\omega\kappa''\vec{E}$, as illustrated in equation 2.6.

$$\vec{\nabla} \times \vec{H} = \sigma\vec{E} + \omega\kappa''\vec{E} + j\varepsilon_0\varepsilon_r\vec{E} \qquad (2.6)$$

$$\vec{\nabla} \times \vec{H} = j\omega(\varepsilon_0\varepsilon_r - j\frac{\sigma+\omega\kappa''}{\omega})\vec{E} \qquad (2.7)$$

$$\vec{\nabla} \times \vec{H} = j\omega(\varepsilon_0\varepsilon_r - j\frac{\sigma_e}{\omega})\vec{E} \qquad (2.8)$$

The effective conductivity is stated as $\sigma_e = \sigma+\omega\kappa''$, and the equation 2.8 is able to be written as follows;

$$\vec{\nabla} \times \vec{H} = j\omega(\varepsilon' - j\varepsilon'')\vec{E} \qquad (2.9)$$

In equation 2.9, ε' is defined as $\varepsilon_0\varepsilon_r$, while ε'' is defined as $\frac{\sigma_e}{\omega}$. The variation in ε_r and the variation in σ_e will be examined in this thesis. According to the definitions of permittivity and conductivity, the relative permittivity and effective permittivity of a substance are determined by its molecular structure. Thus, a variation in the dielectric characteristics of tissues indicates changes in the molecular structure of the tissue [46, 47, 48]. Narrowband resonance methods are better suited to monitor slight changes in BGLs and the associated changes in dielectric characteristic. The following formula is an empirical relation between a resonator's effective permittivity and its resonance frequency [43]:

$$f_r = \frac{nc}{L_{eff}\sqrt{\varepsilon_{eff}}} \qquad (2.10)$$

If a resonator has more than one resonance frequencies, the regarded number of the f_r is n; for example, if the resonator is running in dual-mode and the operator is studying the second mode, n should be 2. The equation establishes a clear link between the ε_r of the dielectric medium and the resonator's characteristic response.

2.2 Development of a model dependent on glucose content

Variations in the propagation speed of EM waves in a medium containing biological tissue are translated into a measurable signal by microwave biosensors. The transducer, on the other hand, is unable of identifying whether the variations in permittivity are caused by a protein change or a variation in BGL. Hence, models that characterize a material's permittivity throughout a frequency spectrum are necessary [44]. The frequency-dependent relative permittivity of material has complex form

$$\varepsilon(\omega) \ = \ \varepsilon'(\omega) \ + \ j\varepsilon''(\omega) \tag{2.11}$$

In the presence of EM field, the storage and loss of energy in the MUT are induced by $\varepsilon'(\omega)$ and $\varepsilon''(\omega)$. In [45], the dependence dielectric permittivity on the concentration of solute glucose has been expressed by the molar increment δ and is given by

$$\varepsilon_g \ (\omega) \ = \ [\varepsilon_0 \ '(\omega) + c\delta'] - j[\varepsilon_0 \ ''(\omega) + c\delta''] \tag{2.12}$$

where $\varepsilon_0(\omega)$ is the complex permittivity of DI water ($\varepsilon'(\omega) = 77.23$ and $\varepsilon_0''(\omega) = 15.72$ at 3.6 GHz, 25°C), c is the concentration of glucose, $\delta \ = \ \delta' - \delta''$ is the increase in permittivity when the glucose concentration is raised by 1 unit ($\delta' = 0.00577$ (mg/dL)$^{-1}$ and $\delta'' = 0.00015$ (mg/dL)$^{-1}$). Here the complex dielectric permittivity of DI water has been given by the Havriliak–Negami relaxation model:

$$\varepsilon_0 \ (\omega) = \varepsilon_\infty + \frac{\Delta\varepsilon}{(1+(j\omega\tau)^\alpha)^\beta} \tag{2.13}$$

where $0 \leq \alpha,\ \beta \leq 1$, $\varepsilon_\infty = 4$ is the permittivity in the high frequency limit, $\varepsilon_S \ = 72$ is the static, low frequency permittivity ($\Delta\varepsilon \ = \ \varepsilon_S \ - \ \varepsilon_\infty$), and $\tau \ = \ 10^{-12}$ s is the characteristic relaxation time of DI water at 3.6 GHz. In special cases when $\alpha = 1$, $\beta = 1$; $\alpha \neq 1$, $\beta = 1$ and $\alpha = 1$, $\beta \neq 1$ the Eq. (1) describes the Debye, Cole–Cole and Cole–Davidson relaxation models, respectively. The methodology underlying permittivity fluctuation with frequency is explained by Debye's equations [45]. Despite its popularity as a dielectric model, the Debye model doesn't reliably and sufficiently

explain the permittivity of many tissues across a wide frequency spectrum. The Cole-Cole model is far more accurate, and it has lately been utilized to simulate biological tissues as a function of frequency [46].

Chapter 3

Numerical Computation Model for Non-Invasive Blood Glucose Monitoring

3.1 Sensor Element Design

The Hilbert curve is initially presented by Peano in 1890. The Hilbert Curve can keep its footprint size when the iteration order of the curve grows, but the length of the curve rises. Figure 3.1 depicts the first four orders of a Hilbert curve, denoted by the letter H_n, where n is the order number. When the number of order increases, the architecture gets increasingly complicated and densely packed while remaining non-self-intersecting.
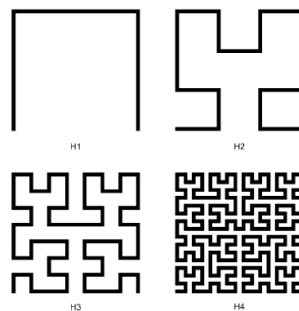
Figure 3.1: The Hilbert Curve from the first to the four orders [47]

A modified 1st order Hilbert-shaped closed curve is modelled as a sensor pattern in [48], due to its periodic and space-filling nature. Figure 3.2 depicts the modified Hilbert-shaped sensor's geometry. A ceramic material has been employed as a

substrate. A slim coating of silver paste has been applied to both the top and bottom of the sensor's ceramic substrate. The width, the length, and the breadth of the curve are represented by h, s, and w, respectively.
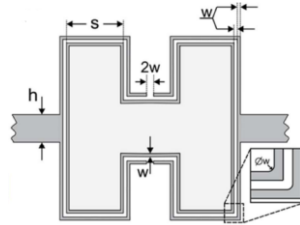
Figure 3.2: The geometry of modified 1st order Hilbert-shaped sensor [48]

In this thesis, the sensor element architecture has been inspired from the modified Hilbert shape used in [48]. To simplify the process of fabrication, this sensor has been optimized by using commonly used microstrip technology. According to the principal of enhancement in sensitivity, the fields need to be strongly limited around the sensing area. So, to obtain high sensitivity and to successfully achieve the concept of highly concentrated energies on the sensing region, the modified Hilbert shaped sensor element has combined with the features of meander line resonator. The 1st form of the microwave sensor element has been designed on FR4 dielectric PCB and has shown in Figure 3.3.

(a)   (b)
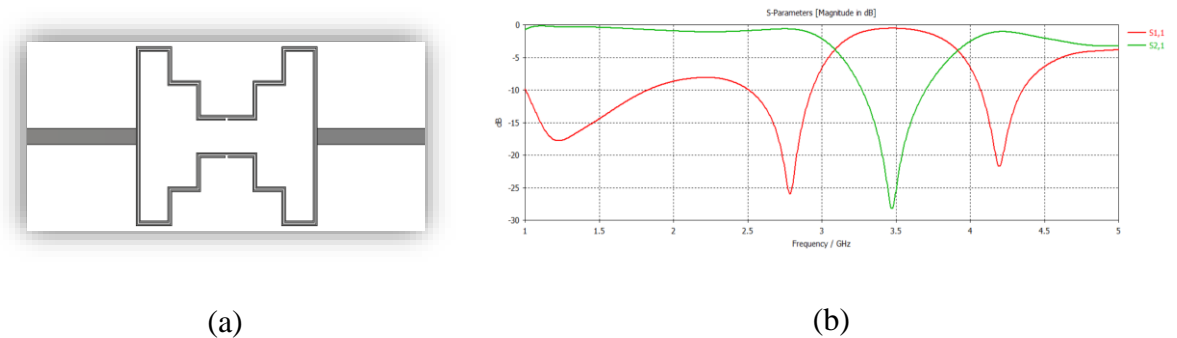
Figure 3.3: (a) The 1st form of the meandered and modified Hilbert shaped sensor element, (b) its S parameter outcomes

In line with the suggestion of the authors in [49], the meandered and modified Hilbert shaped sensor element has been engraved in the PEC, as shown in Figure 3.4. Figure

3.5 represents S_{11} and S_{12} simulation results of the 2nd form of meandered and modified Hilbert shaped sensor element.

(a)   (b)

Figure 3.4: The 2nd form of meandered and modified Hilbert shaped sensor element: (a) lower face (b) the upper face
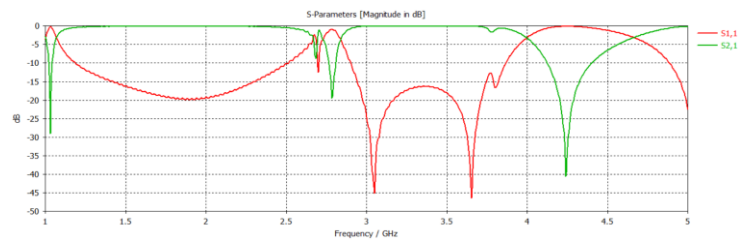
Figure 3.5: The S_{11} and S_{12} simulation results for the 2nd form of meandered and modified Hilbert shaped sensor element

Additional resonators are utilized to improve bandwidth [50]. From this point of view, two asymmetrical microstrip lines are inserted on radiating edges of the sensor in the 1st configuration, as shown in Figure 3.6.

(a)   (b)
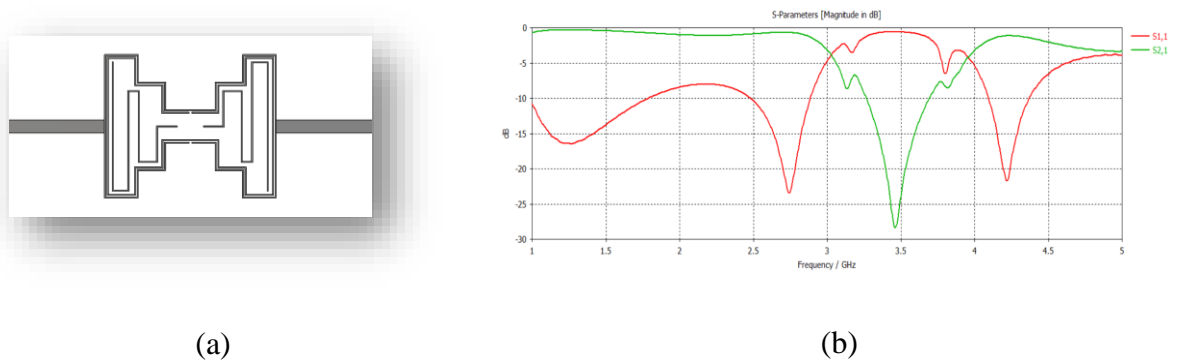
Figure 3.6: (a) The 1st form of the meandered and modified Hilbert shaped sensor element with the additional resonators, (b) its S parameter outcomes

28

In the 2nd form of meandered and modified Hilbert shaped sensor element configuration, microstrip gap has been added to the centre of the upper face of the substrate. Two open ended microstrip lines with a capacitive series coupling between the two ends is shown in Figure 3.7. Figure 3.8 represents S_{11} and S_{12} simulation results of the 2nd form of meandered and modified Hilbert shaped sensor element with the gap on the feeding line.

(a)   (b)
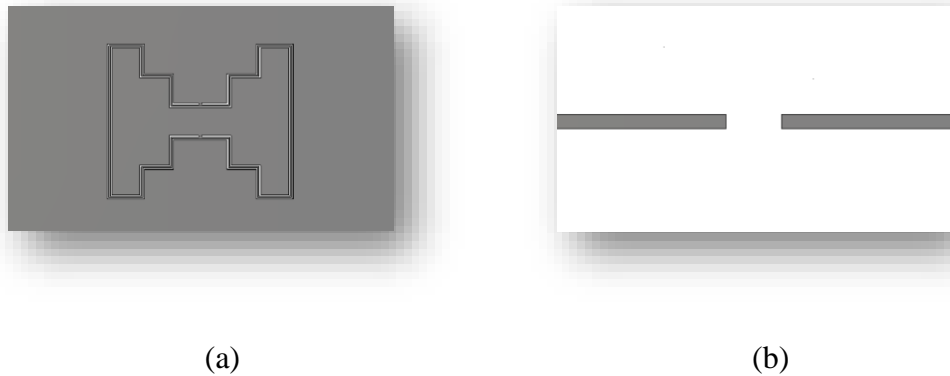
Figure 3.7: The 2nd form of meandered and modified Hilbert shaped sensor element with the gap on the feeding line: (a) lower face (b) the upper face
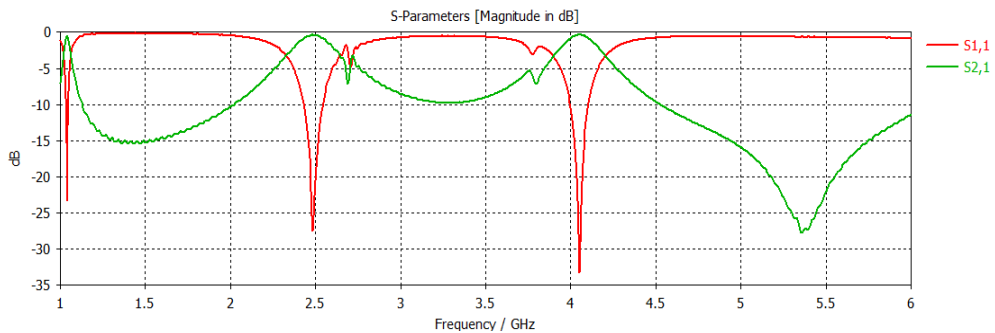
Figure 3.8: The S_{11} and S_{12} simulation results for the 2nd form of meandered and modified Hilbert shaped sensor element with the gap on the feeding line

The thesis has been continued by modifying the 1st form of the microwave sensor element and the following structures have been designed since the 2nd forms of meandered and modified Hilbert shaped sensor element have narrower bandwidth. The S_{11} and S_{12} simulation results with the corresponding structures are given in Figure 3.9
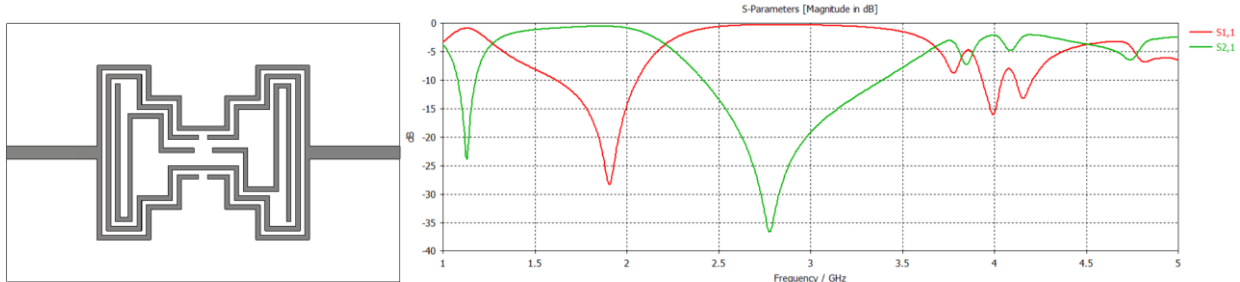
(a)
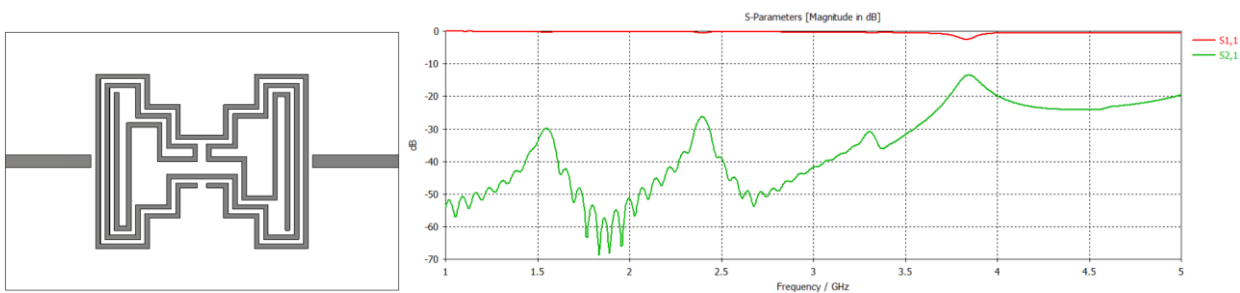
(b)
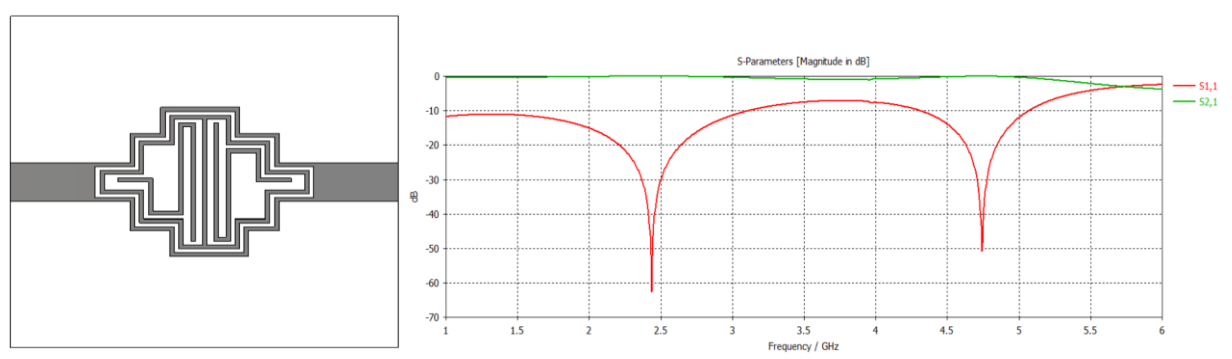
(c)

Figure 3.9: The structure and the S parameter results of: (a) Version 1.1, (b) Version 1.2, and (c) Version 1.3

Version 1.2 has been firstly changed by lowering the capacitive coupling between the two ends. Secondly, more resonators added to the design with and without capacitive coupling. Lastly, the feed lines have been rotated 90° for the design with and without capacitive coupling. The applied changes are respectively shown in Figure 3.10.
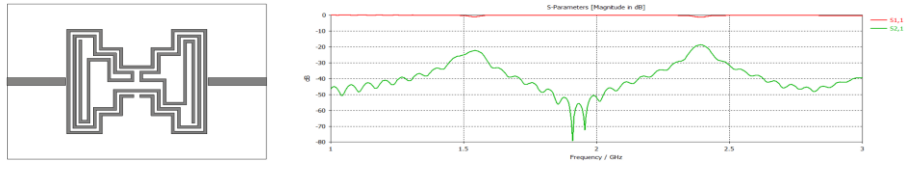
(a)
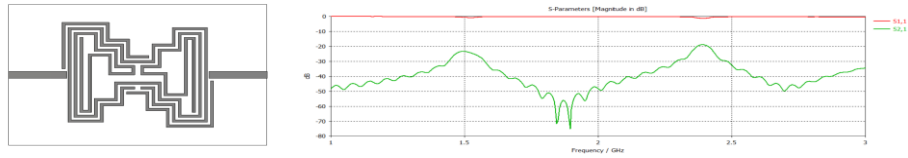
(b)
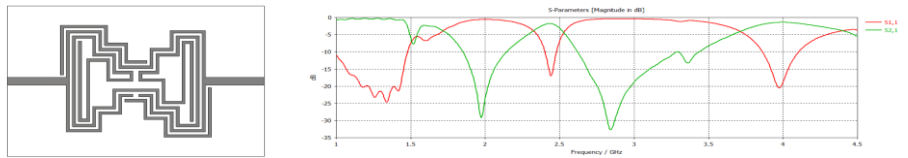
(c)
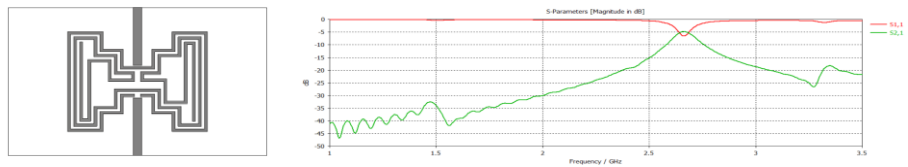
(d)
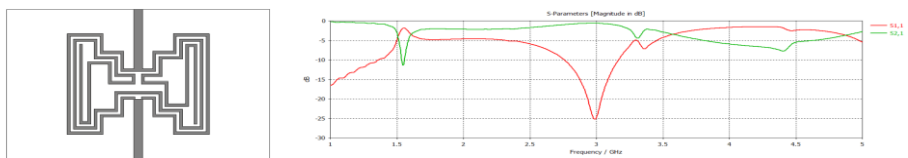
(e)

Figure 3.10: The S parameter results of the structure: (a) lowered capacitive coupling; (b) more resonators with capacitive coupling, and (c) without capacitive coupling; (d) rotated feed lines with capacitive coupling, and (e) without capacitive coupling.

To increase the effect of capacitive coupling, the feed line has been improved by extending the feed line end which is close to the centre of the sensor element. We have already known that thickness and dielectric constant (dc) of the substrate material influences the capacitance of the sensor element considerably. To examine the variation in f_R, the parameters of dc and thickness have been swept using the sensor structure designed in CST MWS. To better understand the results of any change in dc, numerical calculations have been made by changing the value of dc of the substrate, while thickness of the substrate sets to 0.35 mm, 0.5 mm, and 1.7 mm. The S_{11} results for each situation is given in Figure 3.11.
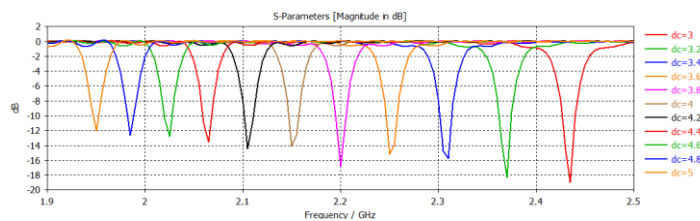
(a)
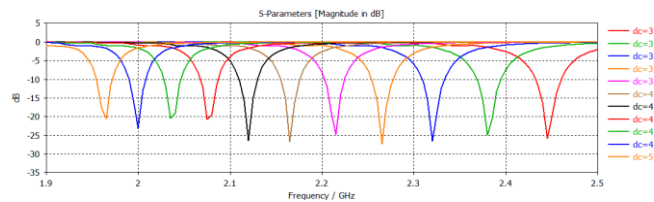
(b)
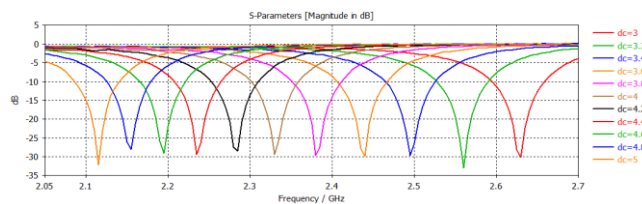
(c)

Figure 3.11: The S_{11} results of the sensor element with respect to the change in dc of the substrate while the thickness of the substrate set to: (a) 0.35 mm, (b) 0.5 mm, and (c) 1.7 mm.

Afterwards, numerical calculations have been made by changing the thickness, while the dc the substrate sets to 3 and 4.4. The reflection coefficients for each situation are given in Figure 3.12.
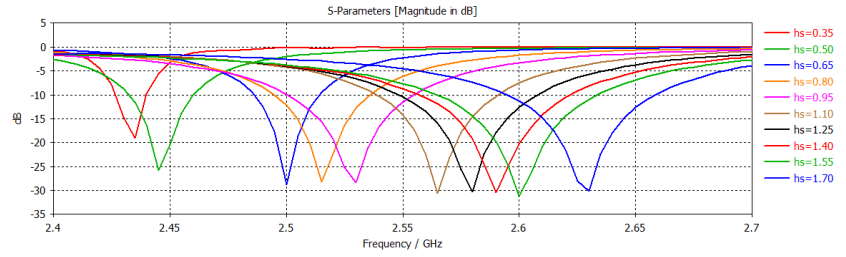
(a)
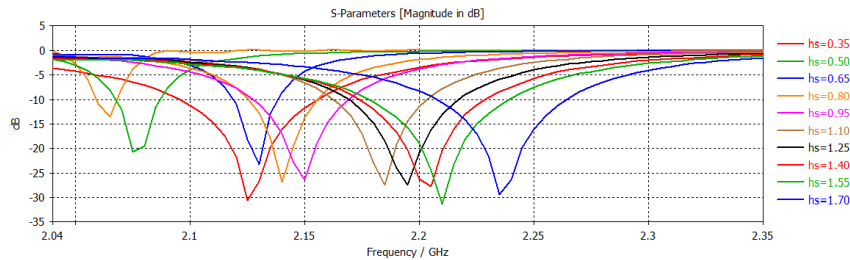
(b)

Figure 3.12: The S_{11} results of the sensor element with respect to change in thickness of the substrate while the dc of the substrate set to: (a) 3 and (b) 4.4.

It can be easily observed that an increase in dc of the substrate reduces f_r of the sensor element, and the f_r rises with an increment in substrate height. Thus, the choice of substrate height and dc of the substrate is critical for the performance of the sensor element. Since substrates also give mechanical support to the sensor element, substrate material should be chosen carefully. Hence, we decided to use Rogers 3003 with the dc of 3.3 and the thickness of 0.501 mm, to attain the f_r to 2.4 GHz which is the operation frequency of XBee modules that will be used in the continuation of the thesis. Figure 3.13 gives the simulation model of this sensor element that have the substrate of Rogers 3003.
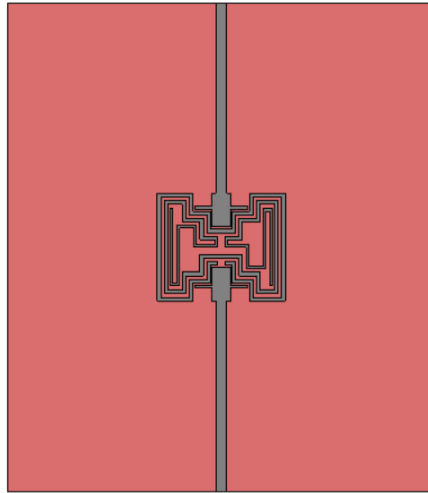
Figure 3.13: The simulation model of the sensor element designed using Rogers 3003

FR-4 is one of the most widely used and the most cost-effective substrates in the fabrication of printed circuit boards. Even though Rogers 3003 gave good results in scattering parameters and frequency, the performance of FR-4 whose thickness is 1.6 mm, the ε_r about 4.4 and the loss tangent about 0.02, has been also tested. The sensor element designed by using FR-4 material is given in Figure 3.14.
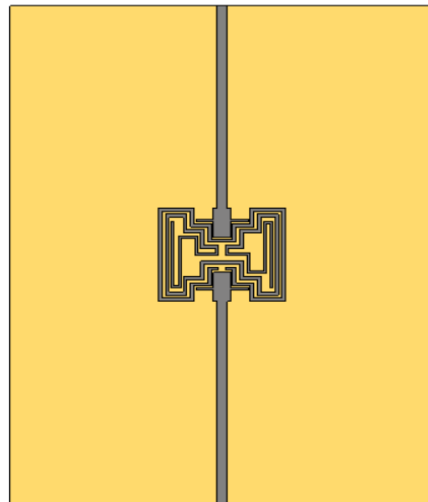
Figure 3.14: The sensor element designed by using FR-4

Thereafter, the sensor element has been continued to optimize since the reflection coefficient of the fabricated sensor element was not as we expected exactly. To optimize the sensor element, the thickness of the feed line of the sensor element has

been swept. It has been observed that the sensor element, as shown in Figure 3.15, gives the best results when the thickness of the feed line is equal to 0.50 mm.
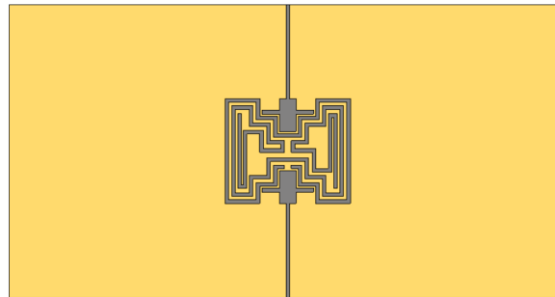
Figure 3.15: The optimized sensor element designed by using FR-4

3.2 Fingertip Models

At a frequency of 1 GHz, a particular wave travelling through skin and fat layers transmits 50% of its intensity, and the same wave going through muscle layer transmits 93% of its intensity. Therefore, if the sensor is put on muscle rather than fat tissues, it will be in contact with more blood. The more blood analyzed, the more precise the measurement. The sensor must be able to sense in dielectric permittivity. The variations occur due to placing a finger on the planar resonator, allowing us to take a measurement with a high degree of energy transfer. According to the literature, any increment in glucose content decreases the ε_r of blood which varies operating frequency [42]. To illustrate the effects of the BGL variation in a fingertip, human tissue models from several articles have been simulated using CST MWS, as depicted in Figure 3.16. The variation of blood permittivity was different for each of the finger models.
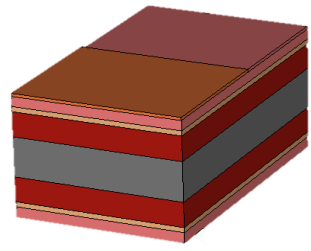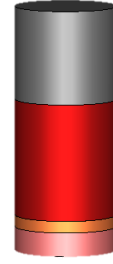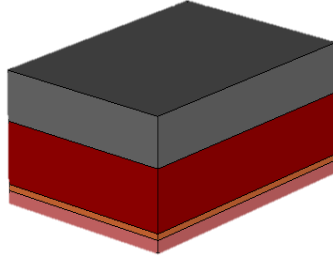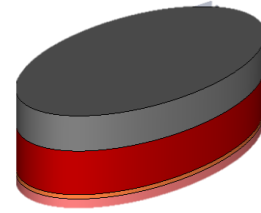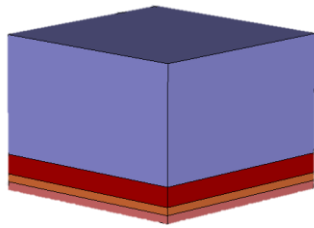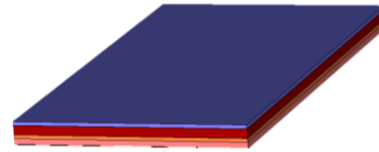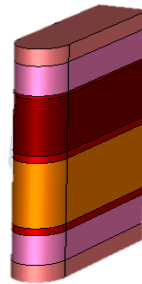
Figure 3.16: The 3D EM illustrations of the fingertips suggested in: (a) [42], (b) [40], (c) [41], (d) [43], (e) [1], (f) [44], and (g) [47]

The authors in [42] claims that the difference between 100 mg/dL and 500 mg/dL is about 0.24. So, the range of the ε_r of blood in the first finger model is between 59 and 59.24, with a step width of 0.06. In [40], the ε_r of blood in the thumb is changed from the hypoglycemia to hyperglycemia, i.e., ε_r values in between 55 and 65. In [41], the

Cole-Cole parameters have been used for each phantom sample. The 2nd order Debye model has been used for the the ε_r of blood in the finger model presented in [43]. The decrement in the f_r is about 4-8 MHz as the permittivity of blood increases. The $\Delta\varepsilon_1$ swept from 30 to 70 in [1], by using the Debye model. This range has been considered to include the differences between 0-16000 mg/dL glucose content in blood. There is no information about the variation of blood permittivity in the articles of [44] and [47]. To illustrate the effects of the BGL variation in a fingertip, the cylindrical fingertip proposed by Sethi et al. [43], has been selected. Its radius and height are 16 mm and 10.5, respectively. The fingertip model composed of four layers which are skin, fat, blood, and bone. After the multi-layer structure has been modelled, the dielectric properties of each layer have been specified by utilizing the single-pole Cole-Cole model parameters at 2.4 GHz [46].

3.3 Effects of Blood Glucose Level Variation in Fingertip

To monitor BGL variations through a fingertip, an insulating layer has been placed between the sensor element and a fingertip. Plexiglass material with the dielectric constant of 3.4 has been selected as an insulating layer. Figure 3.17 gives all the simulation model for the sensor element designed by using Rogers 3003 with plexiglass and the fingertip model, and their scattering parameter results are presented step by step in Figure 3.18.

| (a) | (b) | (c) |
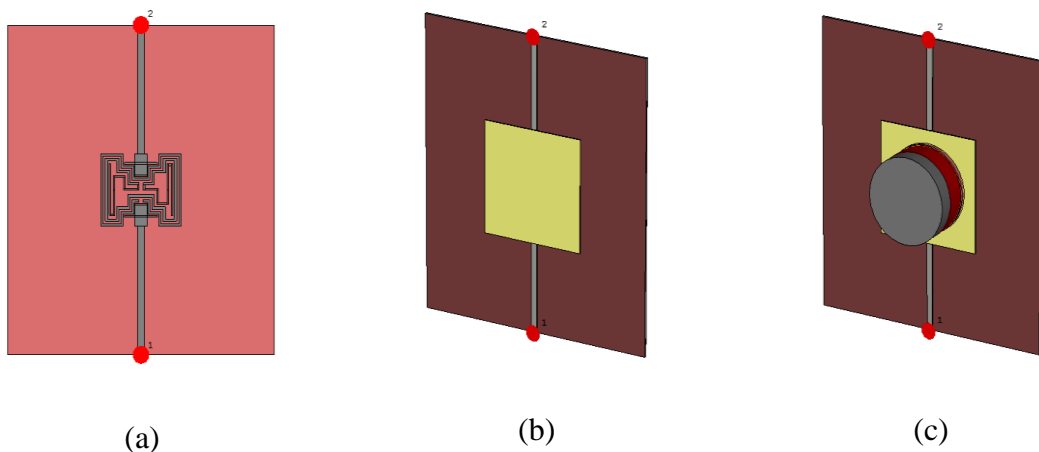
Figure 3.17: (a) The sensor element designed by using Rogers 3003: (b) with plexiglass and (c) with plexiglass and fingertip model
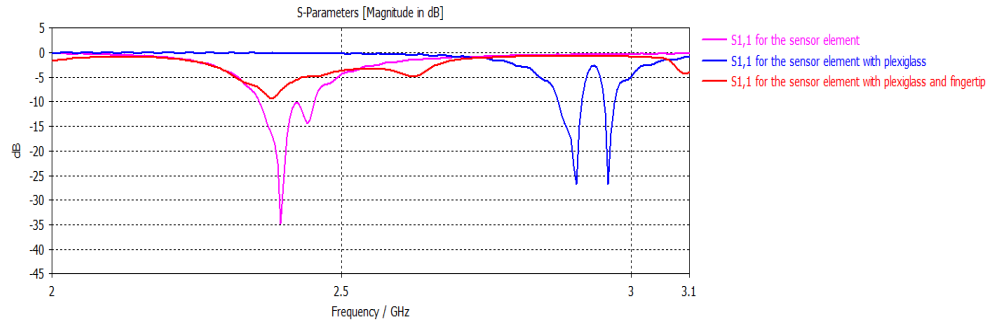
(a)
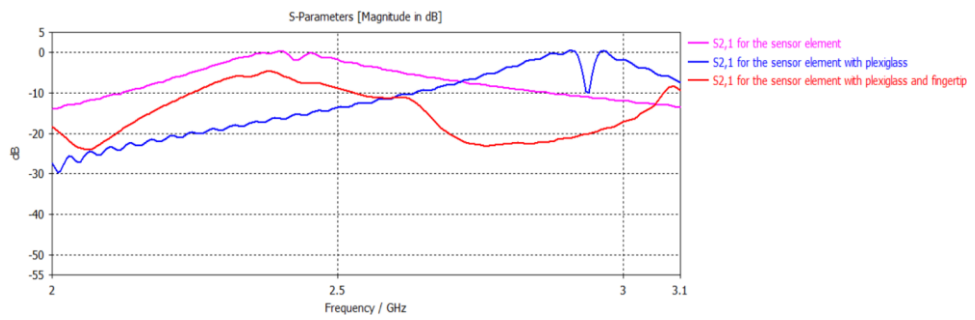
(b)

Figure 3.18: (a) S_{11} and (b) S_{21} of the sensor element designed by using Rogers 3003 with plexiglass and fingertip model

Figure 3.19 gives all the simulation model for the optimized sensor element designed by using FR4 with plexiglass and the fingertip model, and their scattering parameter results are presented step by step in Figure 3.20.
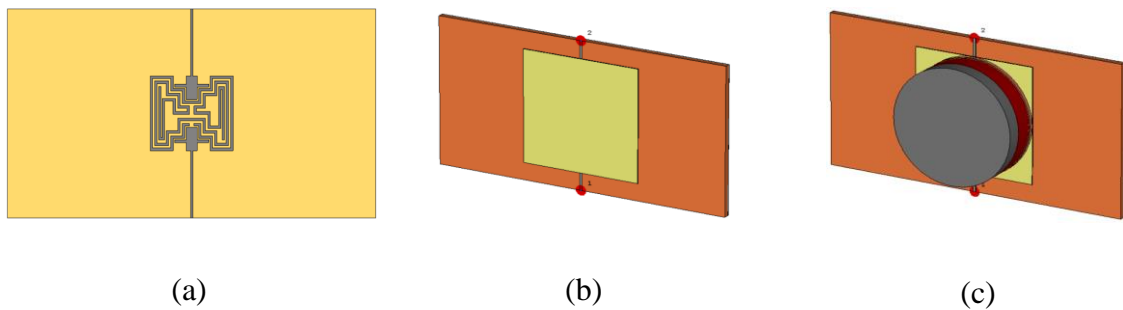
(a)   (b)   (c)

Figure 3.19: (a) The sensor element designed by using FR4: (b) with plexiglass and (c) with plexiglass and fingertip model
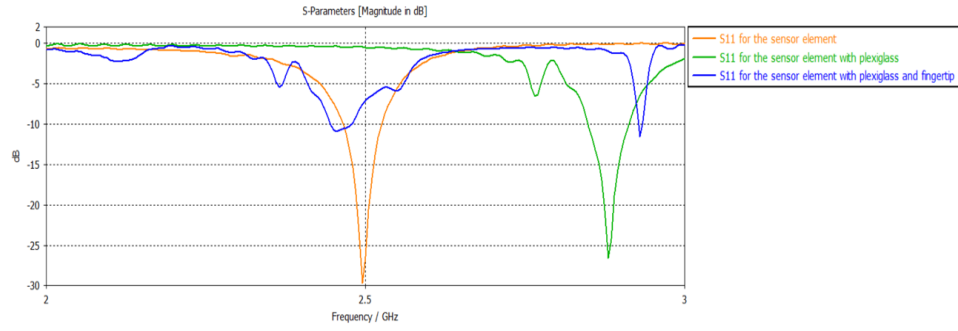
(a)
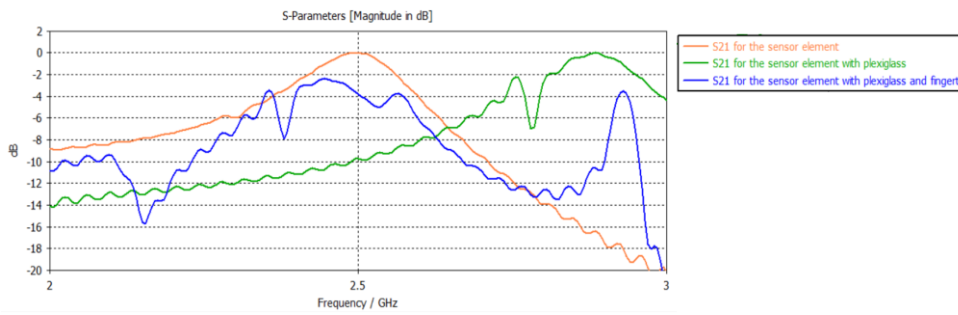
(b)

Figure 3.20: (a) S_{11} and (b) S_{21} of the sensor element designed by using FR4 with plexiglass and fingertip model

A variation in glucose level is caused by a variation in the the ε_r of blood. Therefore, a variation occurs in the relative frequency. The f_r of the sensor element is less than the previous condition that there is no fingertip model. To test the efficiency of the model, simulations have been run by changing the blood permittivity corresponding to the ranges from hypoglycaemia to hyperglycaemia. [51] has been used to determine the dielectric characteristics of blood concerning BGLs. The simulation results, as shown in Figure 3.21, demonstrated that any increase in ε_r lowers the resonant frequency; any increase in the permittivity of blood, drops the resonant frequency by around 5 MHz. It is also noted that when ε_r increases, the reflection coefficient decreases while the transmission coefficient increases.
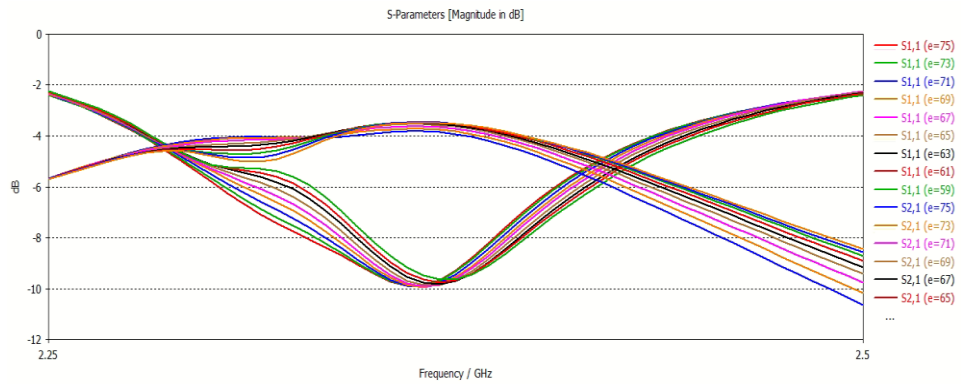
Figure 3.21: The scattering parameters of the optimized sensor element with

plexiglass and fingertip model due to changes in the ε_r of blood

Chapter 4

Experiments for Non-Invasive Blood Glucose Monitoring

4.1 Tissue mimicking phantoms

Phantoms are commonly used to conduct early testing to ensure that antennas and microwave equipment are working properly. Physical phantom characterization is a time-consuming process that involves considering a variety of factors such as operating frequencies, tissue type, shape, width, uniformity, and deterioration [2]. Liquid phantoms are really the easiest and most cost-effective types of physical phantoms. Even though liquid phantoms are useful for establishing a field distribution throughout the body, obtaining data from surface spots is difficult owing to physical constraints. Furthermore, the body is presumed to be homogenous when utilizing liquid phantoms; consequently, liquid phantoms are probably best suited for practicability and other early-stage investigations. Sugar-water phantoms have been postulated for this thesis. The dielectric characteristics of the phantom have been changed by varying the quantity of sugar. Phantoms can be made by dissolving sugar with water. In the scope of this thesis, fifteen liquid phantoms have been prepared. The phantoms included no further chemicals, such as hardening agents or preservatives. The BGL of the phantoms with respect to the sugar concentration and their respective ε_r values are listed in Table 4.1, respectively.

Table 4.1: The BGL of the phantoms and their respective relative permittivity values

Sugar Concentration (gr)	BGL (mg/dl)	ε_r
0	0	70.6300
0.20	200	70.5871
0.50	500	70.5213
1	1000	70.4079
1.5	1500	70.2900
2	2000	70.1674
2.5	2500	70.0401
3	3000	69.9083
3.5	3500	69.7718
4	4000	69.6307
4.5	4500	69.4849
5	5000	69.3345
5.5	5500	69.1795
6	6000	69.0199
6.5	6500	68.8556
7	7000	68.6868
7.5	7500	68.5132
8	8000	68.3351
8.5	8500	68.1523
9	9000	67.9649

From the information in Table 4.1, it can be concluded that ε_r of the solutions decreases by the addition of sugar concentration. This is the result of the change in electrolyte balance in liquid phantoms. It should be also noted that measurements have been recorded in room temperature.

4.2 Experimental Measurements for the Sensor Element

According to the simulation results, it is observed that FR-4 can be used for the sensor element designs. Therefore, the first prototype has been fabricated on FR-4 material with a copper thickness of 35 μm and dielectric substrate thickness of 1.6 mm, by using Eleven Lab PCB Prototyping Machine from Mits. Lastly, 50 Ω connectors heve been placed to two ports of the sensor element. The first fabricated prototype is shown in Figure 4.1.
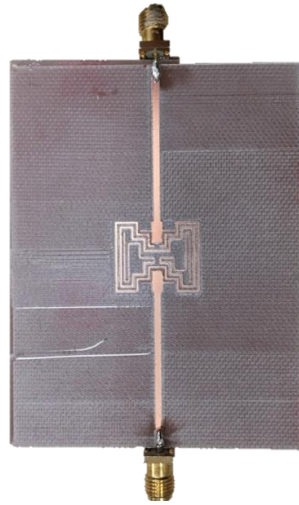
Figure 4.1: The first fabricated sensor element

The performance of the first fabricated prototype has been investigated by performing experiments. The reflection coefficient of the fabricated sensor element has been measured using LibreVNA. The LibreVNA is a two-port, open-source USB-based vector network analyzer. This vector network analyser has two measurement ports that can be used to measure the entire set of reflection and transmission coefficients ($S_{11}/S_{12}/S_{21}/S_{22}$). Although the LibreVNA hardware is intended to be used as a VNA, the general hardware architecture is sufficiently close to that of a spectrum analyser that simple two-channel spectrum measurements can be conducted. The experiment results have been compared with its simulation results, as shown in Figure 4.2.
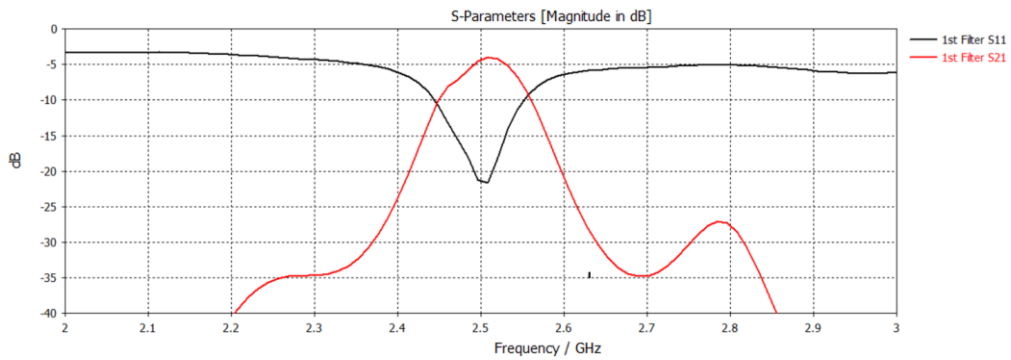
Figure 4.2: The simulation and experiment results for the first fabricated sensor element

Then, the optimized form of the sensor element has been fabricated since the operating frequency of the first fabricated sensor element has not been matched with its simulation result. Therefore, the optimized form of the sensor element has been fabricated, and its performance has been investigated by performing experiments. The fabrication process of the second prototype is the same as the first prototype. The second fabricated prototype is shown in Figure 4.3.
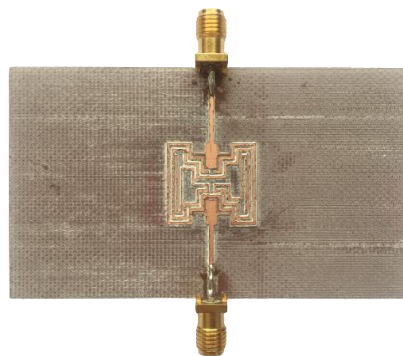
Figure 4.3: The second fabricated sensor element

The reflection coefficient of the second fabricated sensor element has been measured using LibreVNA. Since the measured reflection coefficient of the second fabricated sensor element have been perfectly matched with its simulation result, the experimental process has been continued by measuring the transmission coefficient of the second fabricated sensor element, as shown in Figure 4.4.

(a)   (b)
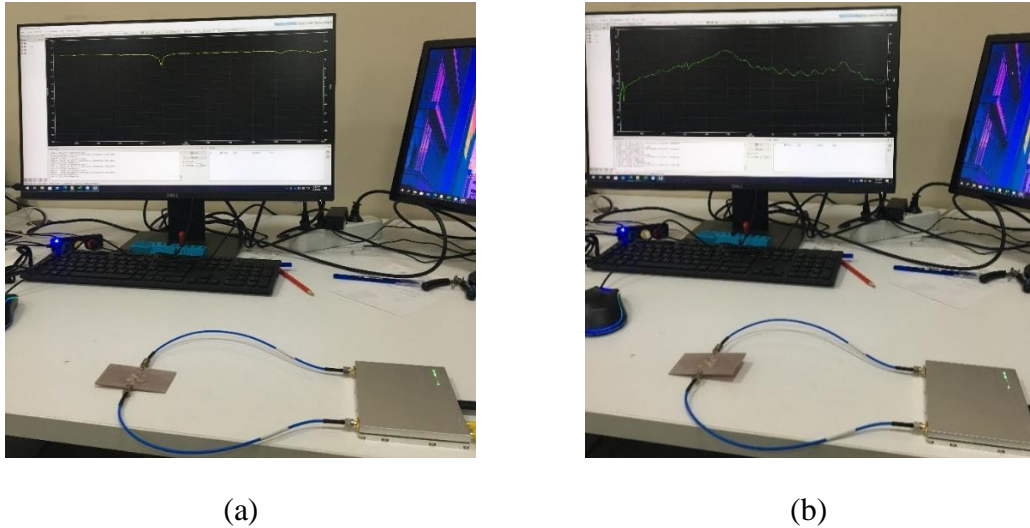
Figure 4.4: The measured (a) reflection coefficient and (b) transmission coefficient
of the second fabricated sensor element by LibreVNA

The numerical analysis and the experimental results of the second fabricated sensor
element have been compared with its simulation results, as shown in Figure 4.5.
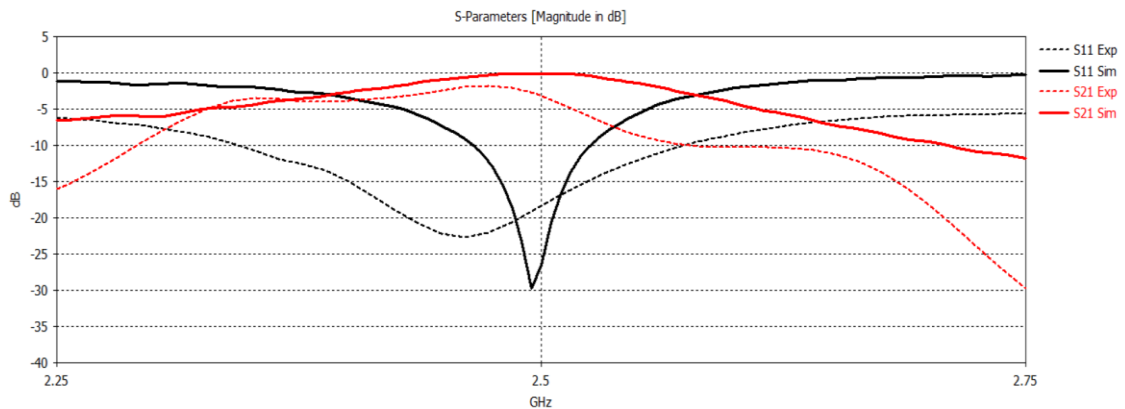
Figure 4.5: The simulation and experiment results for the second fabricated sensor
element

4.3 Experiments with the Tissue Mimicking Phantoms

For the tests with the liquid phantoms that have been already mentioned in Section 4.1.
The reflection coefficient corresponding to the phantoms have been measured using
LibreVNA, in the presence of watery samples on the middle of the sensor element
since the EM waves are centred in the middle section of the sensor element. The

reflection coefficient of the second fabricated sensor element have been recorded, as shown in Figure 4.6.
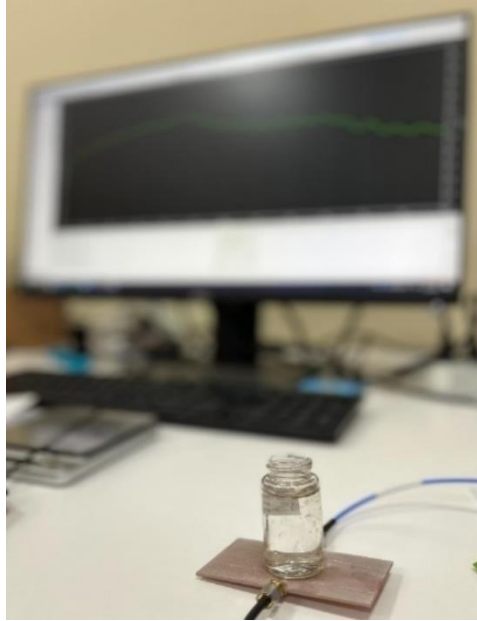
Figure 4.6: The measurement setup for second fabricated sensor element

The transmission coefficient measurements have been performed with respect to the varying sugar concentration in liquid phantoms by using the same setup. The measured S_{11} and S_{21} of the second fabricated sensor element have been given in Figure 4.7. From the experiments, it is easily seen that the S_{11} rises, and the f_r drops, as the sugar content in watery samples rises. The S_{21} behaviors in the opposite way.
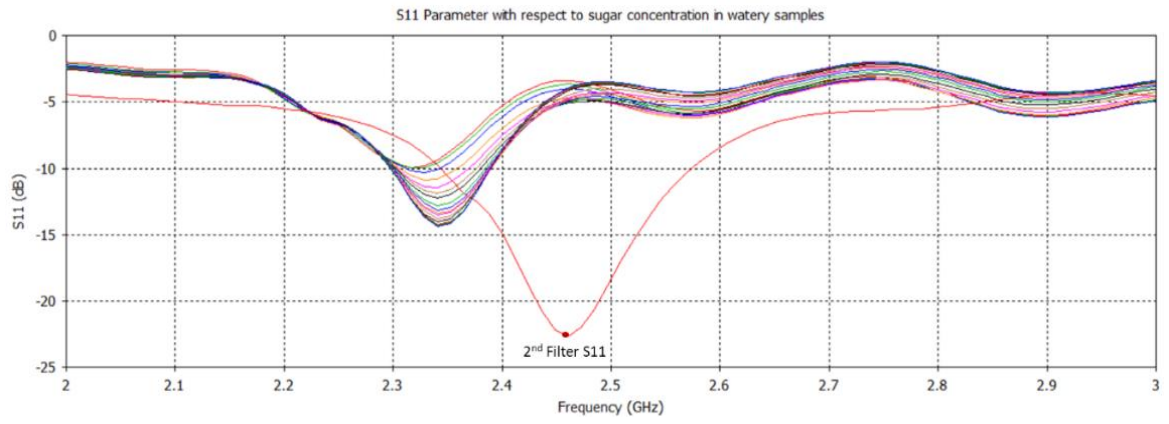
(a)
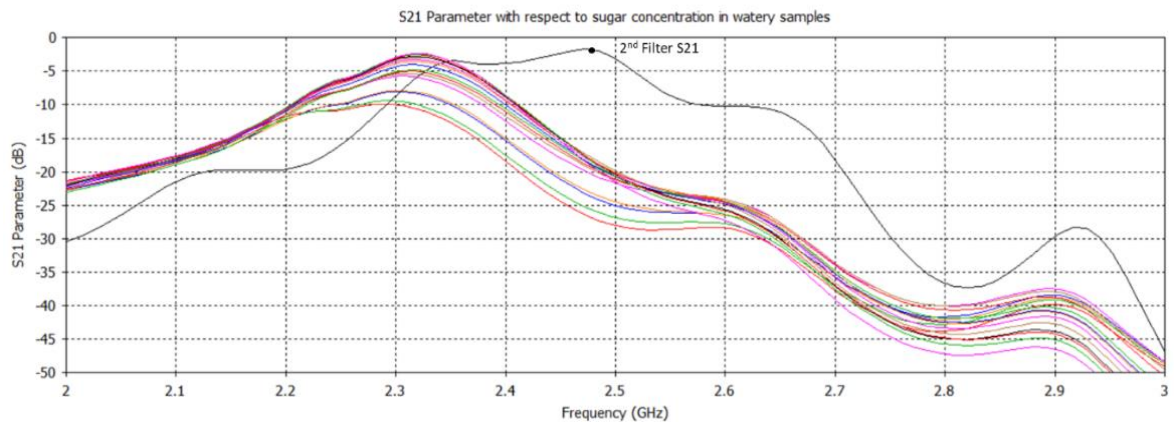
(b)

Figure 4.7: The measured (a) S_{11} and (b) S_{21} of the second fabricated sensor element with watery samples

Chapter 5

Measurement System Hardware and Software

5.1 Measurement System Design

It is critical to enhancing provider capacity so that they can care for more patients without sacrificing quality or overburdening the providers. Many adjustments are recommended to solve the present shortcomings to respond to such a pressing requirement. To deliver accurate and early diagnoses, the future generation of technology must address multiple-device integration and the ability to collect clinically important data, as illustrated in Figure 5.1 [44]. Several efforts have been reported in the literature that focus on economical and portable non-invasive glucose detecting using EM technique. Despite the effort, glucose monitoring has been remained as an unsolved problem.
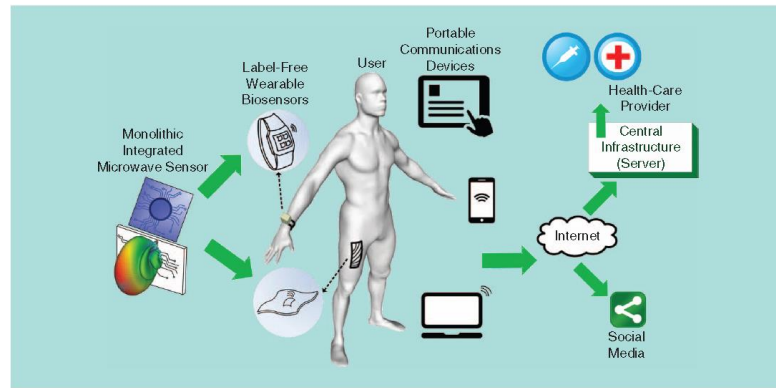
Figure 5.1: A representation of a health monitoring system [44]

A wireless sensor network is a clever solution to the challenge of collecting environmental data. Figure 5.2 shows a schematic depiction of the thesis. Low-power XBee modules can be utilized for wireless communication, allowing a mesh or tree network to be formed within the array of sensors and subsequently data to be transmitted to the gateway node. The XBee network may be set up in either AT or API mode. The AT model is simple to set up, however, there are only two options: Broadcast and Unicast. The API mode must be used to enable the Multicast option. Each API transfer can return a send status frame that indicates whether the transmission succeeded or failed. As a result, RSSI can be acquired from an RX packet in this mode.
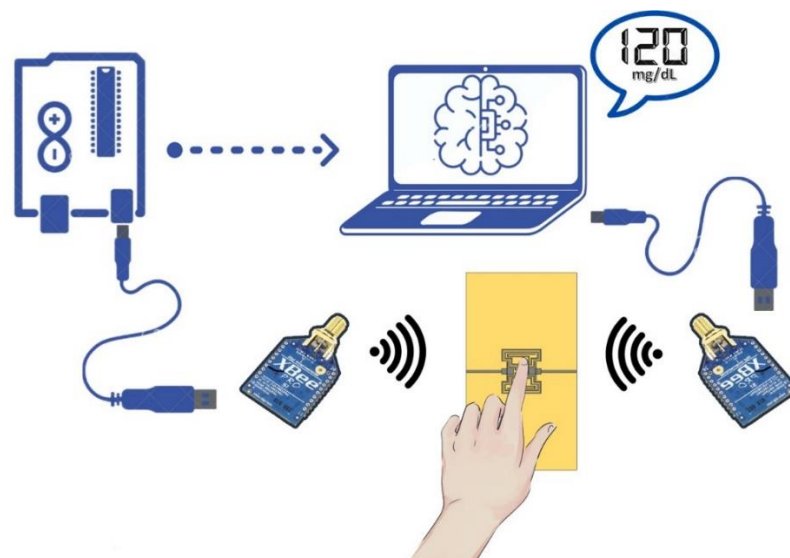
Figure 5.2: The measurement scenario

5.1.1 XBee Configurations

In this thesis, the RSSI power level of XBee module has been validated as an electromagnetic measurement technique. This technique monitors the reduction of the RSSI power level with increasing glucose concentration. RSSI is an estimation of the power of a radio signal received by the receiver antenna. It is measured in decibels per meter and is used to characterize signal intensities for radio and audio frequencies. The Friis transmission equation is the ratio of the received power P_r to the transmission power P_t and it can be expressed as:

$$P_r = P_t \times G_t \times G_r \left(\frac{\lambda}{4\pi d}\right)^2$$

(5.1)

where, G_t, G_r are gain of transmitter and gain of receiver respectively; d is the distance between the sender and receiver. The received signal strength is converted to RSSI which can be defined as the ratio of the received power P_r to the reference power P_{Ref} [52].

$$RSSI = 10 \times log \left(\frac{P_r}{P_{Ref}}\right)$$

(5.2)

For the measurement system, two XBee modules and the Arduino Uno board have been used. In order to get RSSI values to estimate glucose level in blood, the XBee modules has been configured to employ as a receiver and transmitter. The configuration process has been started by downloading XCTU. The program has been run and the XBee modules via XBee Explorer USB boards to a computer have been connected. The "Discover devices" icon has been clicked on the to add XBee modules in the XCTU software, as you can see from Figure 5.3.
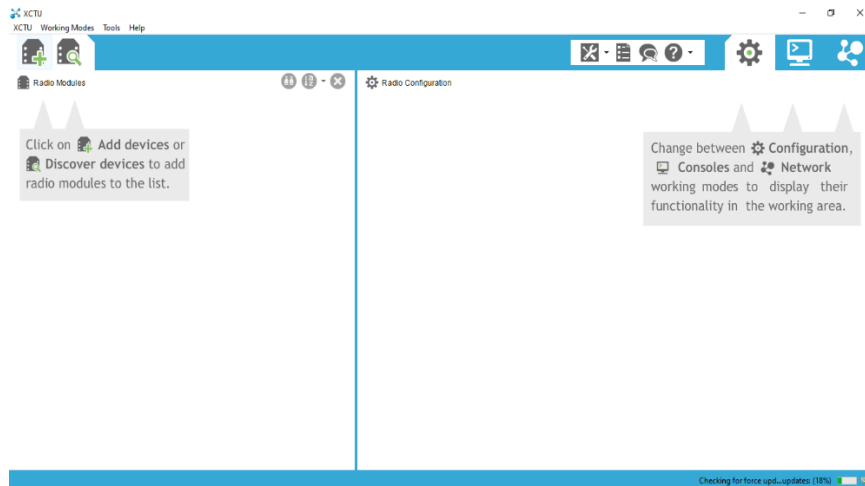
Figure 5.3: XCTU Interface for the configurations

After adding the modules, we set the CH as "C" and the ID as "1001". Both values need to be the same for both of the XBee modules to communicate. Then, we set the firmware version to 802.15.4 and the newest version and put both Xbee modules in API mode 2. The XBee modules installed on the XBee Explorer USB board have been programmed to broadcast a data packet indefinitely, allowing the receiver XBee module attached on the Arduino to receive frequent RSSI value updates. This data packet has been generated using the frame generator. The required settings have been done, as shown in Figure 5.4.
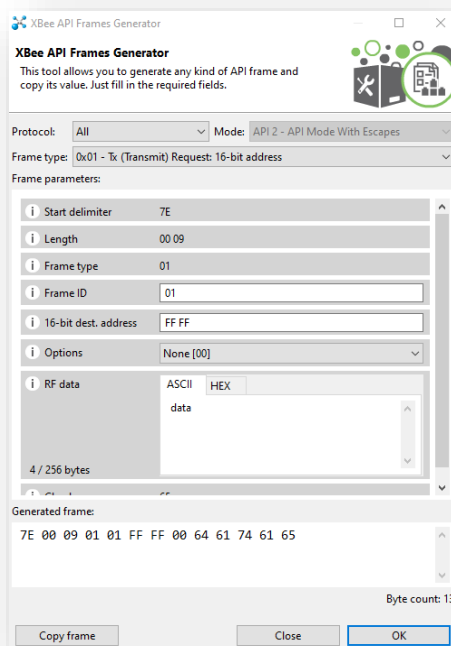
Figure 5.4: XBee API Frame Generator

After data packets have been generated, we checked the connection. As it can be seen from the Figure 5.5. When a XBee module sends a data packet, the other one successfully receives it.
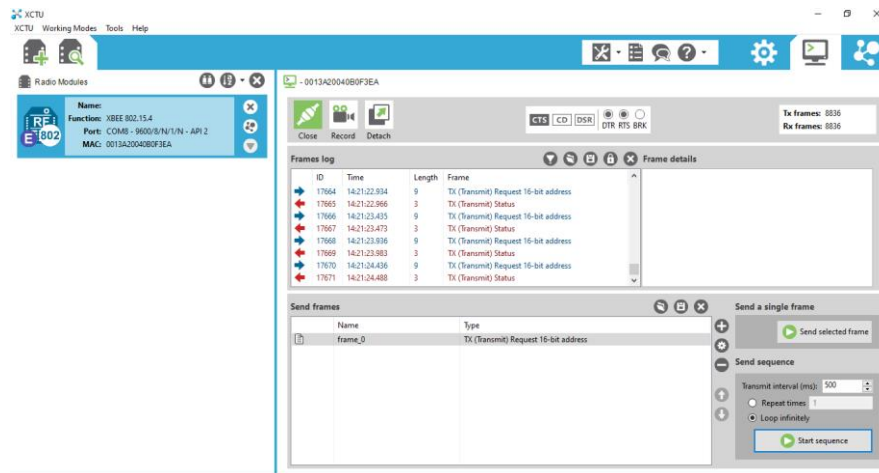
Figure 5.5: API transmission between the XBee modules

5.1.2   Arduino Code

After the XBee modules has been connected to the computer via XBee Explorer USB board and the another has been attached to Arduino, we connected the Arduino Uno to one of our computer's USB ports and opened Arduino IDE. The code in Appendix A, has been implemented. This code controls the packets received by the module connected to Arduino, calculates RSSI and shows on a Serial Monitor an LCD Screen. In other words, we have one XBee send a packet, and the other read the packet and output the RSSI value. The transmitter XBee just send any packet via a X-CTU Software, and the receiver XBee module that is connected to Arduino use to read it. The overall measurement set-up is given Figure 5.6.
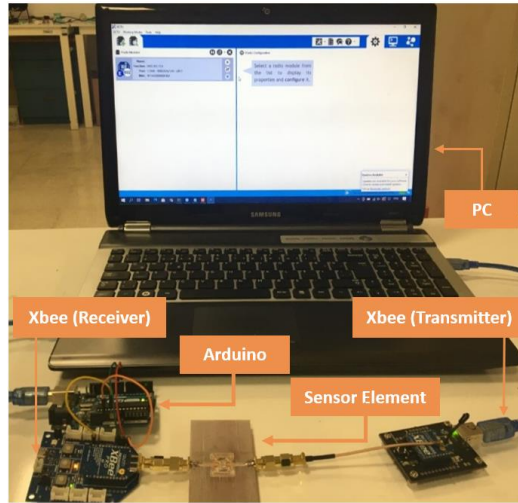
Figure 5.6: The measurement set-up

5.1.3 BGL Estimation via RSSI

Sensors are critical components of contemporary electronics in the twenty-first century. Traditional sensors, on the other hand, are no longer enough. Machine Learning Algorithms have provided several benefits, including the ability to learn and extract characteristics from a dataset. An arbitrary collection of data is the sole condition for the algorithms. The algorithms are based on statistical and mathematical approaches that have been created to investigate processes and, finally, extract critical information from any dataset. As it has been mentioned earlier, a change in RSSI may be utilized to estimate a variation of glucose content in blood. Once the wireless communication has been succeeded, python code in Appendix B has been developed to detect changes in RSSI that defines change in glucose concentration in blood. The developed machine learning code includes four supervised learning algorithms and six ensemble algorithms: SVR, DTR, PR, RFR, BR, ABR, XGB Regressor, GBM, LGB Regressor, and CBR. The code shows and plots the captured RSSI values in real time.

First, we started to build our model by adding the necessary libraries. The .csv file required to train the Machine Learning model has been generated using data from the experiments performed. If we take a look at our data, we can easily observe that it consists of 2 columns named RSSI values and relative permittivity of the blood. 214 data obtained from experimental results have been used in the training of the models. Model performance has been tested with 214 data that have not been in the training

data. The algorithm is developed in python by utilizing the interface of Spyder. Consequently, ε_r of the blood with respect to the BGL has been estimated in real time using the data containing the RSSI values from the receiver XBee module via the Serial Port, connected to Arduino. This study shows that when the dielectric constant of a liquid phantom, or the glucose content in a liquid phantom, increases, so do the RSSI values. The estimation models have been compared with the regression metrics R^2, MSE, MAE, RMSE. The results of the performance analysis are given in Fig.5.7 and Fig. 5.8.
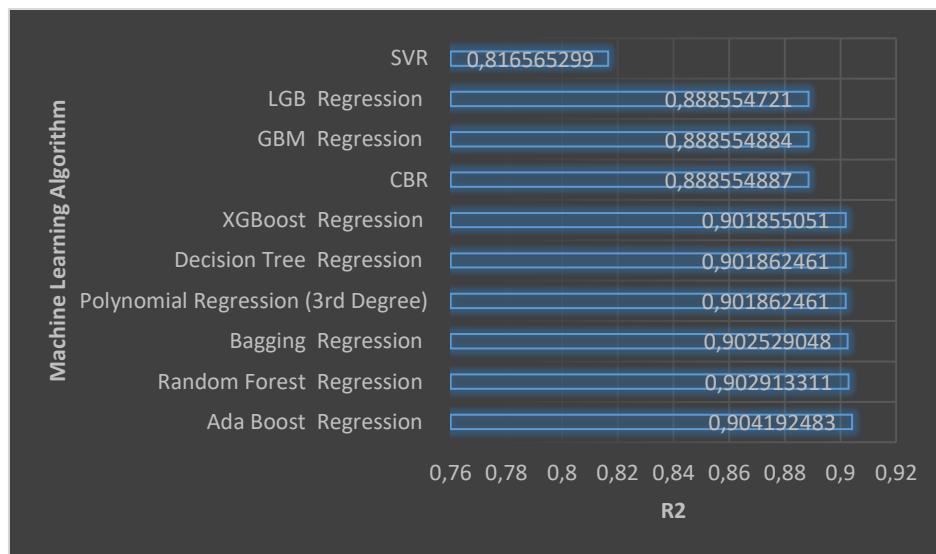
(a)
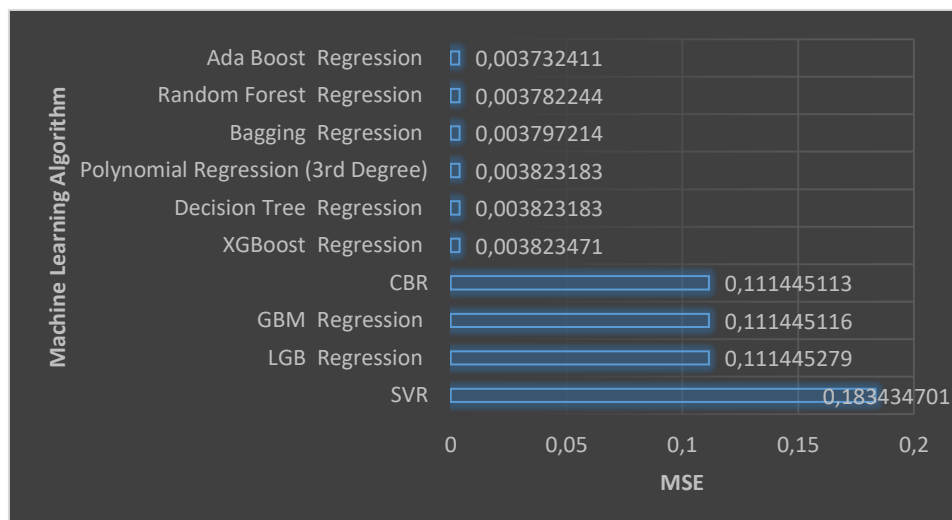
(b)

Figure 5.7: The performance of the estimation models with respect to: (a) R^2 and (b) MSE
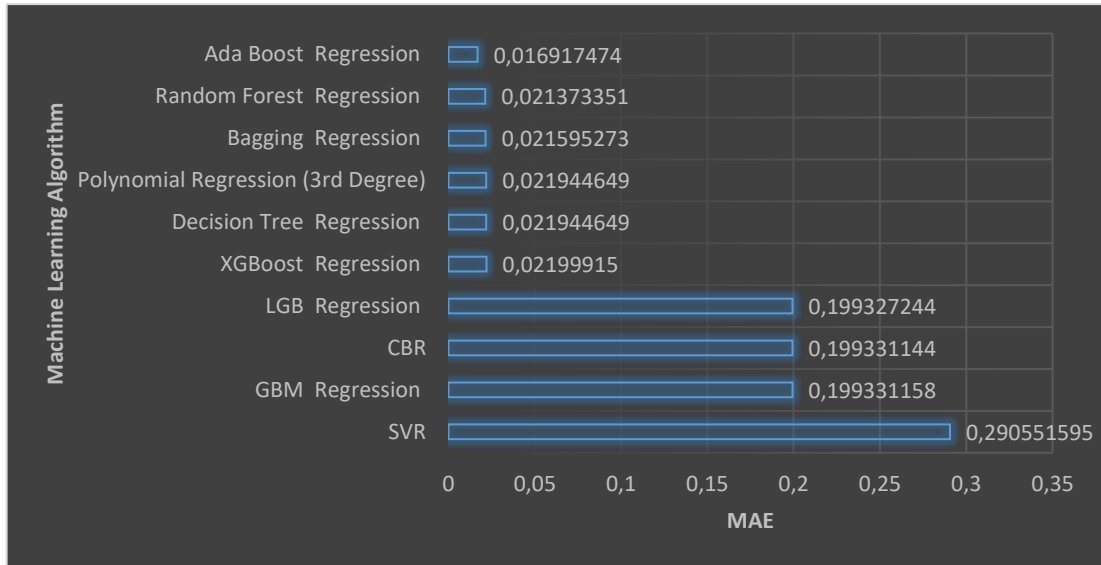
(a)
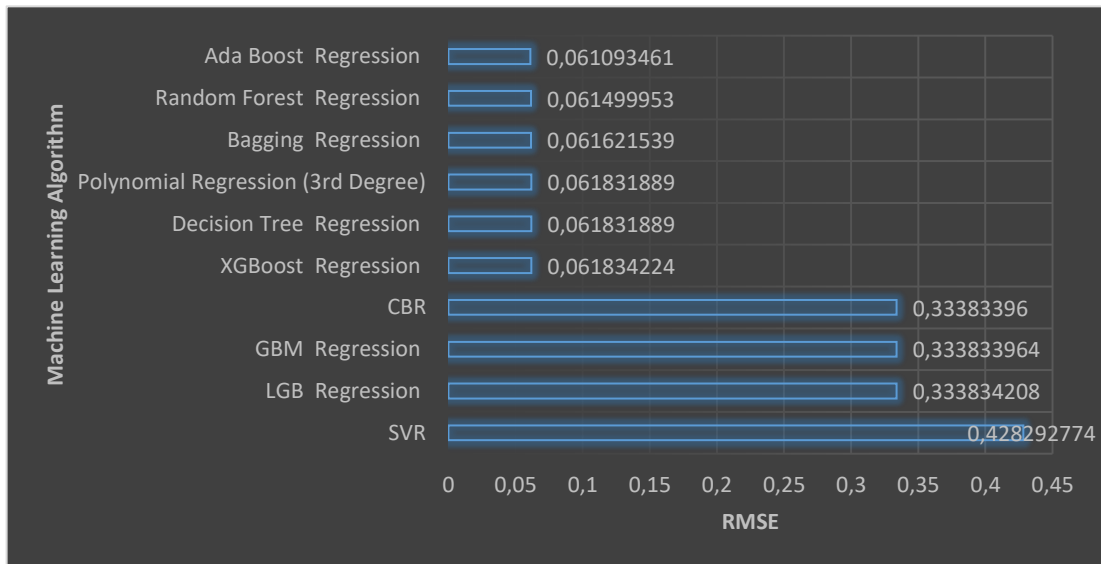
(b)

Figure 5.8: The performance of the estimation models with respect to: (a) MAE and
(b) RMSE

Chapter 6

Conclusion and Future Works

The designed sensor unit structure is primarily inspired from the modified Hilbert shape. to obtain high sensitivity and to successfully achieve the concept of highly concentrated energies on the sensing region, Hilbert shaped sensor unit has modified by adding more resonators and a capacitive coupling. The sensor unit has been simulated by using the electromagnetic simulation tool of CST MWS to model the designed sensor unit and monitor BGL variations through the fingertip which has already been published, considering physiological and electrical properties of a human fingertip. Additionally, an insulating layer has been placed between the sensor unit and the fingertip. Plexiglass material with the dielectric constant of 3.4 has been selected as an insulating layer. The proposed sensor element operates at 2.495 GHz with the S_{11} of -29.72 dB and the S_{21} of -0.049 dB in air, and 2.88 GHz with the magnitude of S_{11} -26.60 dB and the S_{21} of -0.011 dB in the case of there is a plexiglass on the sensor unit. To constitute a link between the response of the sensor element and BGL variation in the fingertip, the sensor unit has been simulated by changing the blood permittivity corresponding to the ranges from hypoglycaemia to hyperglycaemia. The outcomes of the simulations are showed that any increase in ε_r lowers the resonant frequency; any increase in the permittivity of blood, drops the resonant frequency by around 5 MHz. It is also noted that when ε_r increases, the reflection coefficient decreases while the transmission coefficient increases. Once the desired electrical properties for the sensor unit has been achieved, the first prototype has been manufactured. After the performance test of the first fabricated prototype, we decided to optimize it. Hence, the optimized sensor unit has been manufactured as a second fabricated prototype. The S_{11} and S_{21} of the second fabricated sensor unit has been measured using LibraVNA. In a measurement system, there is a loss with the amount -2.82 dB, caused by the coaxial cables. This loss is extracted from the experimental

56

results. As a result of the measurements, it is found that the experimental results and simulation results are matched. Next, tests with tissue mimicking phantoms have been performed using a cylindrical glass container which is filled with sugar-water phantoms. From the experiments, it is easily seen that the S_{11} rises, and the f_r drops, as the sugar content in watery samples rises. The S_{21} behaviors in the opposite way. Finally, a measurement system to implement the non-invasive sensor has been designed. The measurement system has one XBee send a packet, and the other read the packet and output the RSSI value. The transmitter XBee just send any packet via a X-CTU Software, and the receiver XBee module that is connected to Arduino use to read it. The results show that the RSSI values and the observed glucose concentration as a function of the sample's dielectric constant. This thesis also shows that when the dielectric constant of a liquid phantom, or the glucose content in a liquid phantom, increases, so do the RSSI values. Consequently, the simulated results have been sustained by experimental results. Additionally, a machine learning code has been developed to estimate BGL via the S-parameters (S_{11}, S_{21}). The accuracy of the developed code has been evaluated by using the most popular regression metric, R2. This evaluation indicated that BR method is most promising for estimating the BGL, followed closely by the Random Forest Regressor for both scattering parameters. Hence, it is difficult to perform non-invasive in vivo tests for BGL detection due to the other vital signs such as hearth rate, temperature, blood pressure, respiration rate, and many other environmental variables that can influence the response of a microwave device. Therefore, variations in external parameters should be recorded and their effects need to be determined as well. After that, the response of the resulting non-invasive microwave device may be adjusted with respect to the established vital and exterior factors. A second further study on different individuals to acquire real-time data, classified by age, gender, weight, and other parameters. The data need to be cross-referenced with the patient's BGL and health concerns. This may be incorporated into the calibration program. Finally, for a wearable device application, the microwave device's design can be miniaturized and extendable.

References

[1]   W. T. Sethi, M. A. Ashraf, S. A. Alshebeili, and K. Issa, "Thumb positioning analysis of new elliptical-shaped microwave sensors for non-invasive glucose monitoring," *Electronics Letters*, vol. 54, no. 9, pp. 553–554, May 2018, doi: 10.1049/el.2018.0128.

[2]   Tuba Yilmaz, "Wearable RF Sensors for Non-Invasive Detection of Blood-Glucose Levels," London, 2013.

[3]   A. Alzaid, C. Schlaeger, and R. Hinzmann, "6(th) Annual Symposium on Self-Monitoring of Blood Glucose (SMBG) Applications and Beyond, April 25–27, 2013, Riga, Latvia," *Diabetes Technology & Therapeutics*, vol. 15, no. 12, pp. 1033–1052, Dec. 2013, doi: 10.1089/dia.2013.0260.

[4]   Masab Ahmad, Awais Kamboh, and Ahmed Khan, "Non-invasive blood glucose monitoring using near-infrared spectroscopy," 2013.

[5]   A. Tura, A. Maran, and G. Pacini, "Non-invasive glucose monitoring: Assessment of technologies and devices according to quantitative criteria," *Diabetes Research and Clinical Practice*, vol. 77, no. 1, pp. 16–40, Jul. 2007, doi: 10.1016/j.diabres.2006.10.027.

[6]   J. A. Tamada *et al.*, "Noninvasive Glucose Monitoring," *JAMA*, vol. 282, no. 19, p. 1839, Nov. 1999, doi: 10.1001/jama.282.19.1839.

[7]   Diabetes Research in Children Network (DirecNet) Study Group, "Accuracy of the GlucoWatch G2 Biographer and the Continuous Glucose Monitoring System During Hypoglycemia," *Diabetes Care*, vol. 27, no. 3, pp. 722–726, Mar. 2004, doi: 10.2337/diacare.27.3.722.

[8]   David Mendosa, "The GlucoWatch Biographer," 2007. http://www.mendosa.com/glucowatch.htm (accessed Dec. 26, 2021).

[9]   Dongmin Guo, D. Zhang, and Naimin Li, "Monitor blood glucose levels via breath analysis system and Sparse Representation approach," in *2010 IEEE Sensors*, Nov. 2010, pp. 1238–1241. doi: 10.1109/ICSENS.2010.5690611.

[10]   O. S. Khalil, "Non-Invasive Glucose Measurement Technologies: An Update from 1999 to the Dawn of the New Millennium," *Diabetes Technology & Therapeutics*, vol. 6, no. 5, pp. 660–697, Oct. 2004, doi: 10.1089/dia.2004.6.660.

[11]   K. v. Larin, M. S. Eledrisi, M. Motamedi, and R. O. Esenaliev, "Noninvasive Blood Glucose Monitoring With Optical Coherence Tomography," *Diabetes Care*, vol. 25, no. 12, pp. 2263–2267, Dec. 2002, doi: 10.2337/diacare.25.12.2263.

[12]   S. Yeh, C. F. Hanna, and O. S. Khalil, "Monitoring Blood Glucose Changes in Cutaneous Tissue by Temperature-modulated Localized Reflectance Measurements," *Clinical Chemistry*, vol. 49, no. 6, pp. 924–934, Jun. 2003, doi: 10.1373/49.6.924.

[13]   E. B. Hanlon *et al.*, "Prospects for *in vivo* Raman spectroscopy," *Physics in Medicine and Biology*, vol. 45, no. 2, pp. R1–R59, Feb. 2000, doi: 10.1088/0031-9155/45/2/201.

[14]   Y. Shen *et al.*, "Measurement of the optical absorption coefficient of a liquid by use of a time-resolved photoacoustic technique," *Applied Optics*, vol. 39, no. 22, p. 4007, Aug. 2000, doi: 10.1364/AO.39.004007.

[15]   A. Domschke *et al.*, "Holographic sensors in contact lenses for minimally-invasive glucose measurements," in *Proceedings of IEEE Sensors, 2004.*, pp. 1320–1323. doi: 10.1109/ICSENS.2004.1426425.

[16]   Y. Hayashi, L. Livshits, A. Caduff, and Y. Feldman, "Dielectric spectroscopy study of specific glucose influence on human erythrocyte membranes," *Journal of Physics D: Applied Physics*, vol. 36, no. 4, pp. 369–374, Feb. 2003, doi: 10.1088/0022-3727/36/4/307.

[17] T. A. Hillier, R. D. Abbott, and E. J. Barrett, "Hyponatremia: evaluating the correction factor for hyperglycemia," *The American Journal of Medicine*, vol. 106, no. 4, pp. 399–403, Apr. 1999, doi: 10.1016/S0002-9343(99)00055-8.

[18] A. (Zurich, C. Caduff and Y. (Jerusalem, I. Feldman, "Method and a device for measuring glucose," 2007

[19] E. Topsakal, T. Karacolak, and E. C. Moreland, "Glucose-dependent dielectric properties of blood plasma," in *2011 XXXth URSI General Assembly and Scientific Symposium*, Aug. 2011, pp. 1–4. doi: 10.1109/URSIGASS.2011.6051324.

[20] J.-H. Park, C.-S. Kim, B.-C. Choi, and K.-Y. Ham, "The correlation of the complex dielectric constant and blood glucose at low frequency," *Biosensors and Bioelectronics*, vol. 19, no. 4, pp. 321–324, Dec. 2003, doi: 10.1016/S0956-5663(03)00188-X.

[21] V. Rymanov, M. Palandoken, S. Lutzmann, B. Bouhlal, T. Tekin, and A. Stohr, "Integrated photonic 71–76 GHz transmitter module employing high linearity double mushroom-type 1.55 μm waveguide photodiodes," in *2012 IEEE International Topical Meeting on Microwave Photonics*, Sep. 2012, pp. 253–256. doi: 10.1109/MWP.2012.6474105.

[22] V. R. A. S. T. T. M. Palandöken, "Compact metamaterial-based bias tee design for 1.55 μm waveguide-photodiode based 71–76GHz wireless transmitter," *Progress in Electromagnetics Research Symposium*, 2012.

[23] M. Palandoken and H. Henke, "Fractal negative-epsilon metamaterial," in *2010 International Workshop on Antenna Technology (iWAT)*, Mar. 2010, pp. 1–4. doi: 10.1109/IWAT.2010.5464790.

[24] M. Palandoken and H. Henke, "Fractal spiral resonator as magnetic Metamaterial," in *2009 Applied Electromagnetics Conference (AEMC)*, Dec. 2009, pp. 1–4. doi: 10.1109/AEMC.2009.5430645.

[25] S. A. PALANDOKEN M., "Compact Metamaterial Based Bandstop Filter," *MICROWAVE JOURNAL*, vol. 57, no. 10, pp. 76–80, 2014.

[26] M. Palandöken and M. H. B. Uçar, "Compact metamaterial-inspired band-pass filter," *Microwave and Optical Technology Letters*, vol. 56, no. 12, pp. 2903–2907, Dec. 2014, doi: 10.1002/mop.28724.

[27] M. Palandoken, "Metamaterial-Based Compact Filter Design," in *Metamaterial*, InTech, 2012. doi: 10.5772/35853.

[28] C. Gocen and M. Palandoken, "Machine Learning Assisted Novel Microwave Sensor Design for Dielectric Parameter Characterization of Water–Ethanol Mixture," *IEEE Sensors Journal*, vol. 22, no. 3, pp. 2119–2127, Feb. 2022, doi: 10.1109/JSEN.2021.3136092.

[29] S. Mosbah *et al.*, "Compact and Highly Sensitive Bended Microwave Liquid Sensor Based on a Metamaterial Complementary Split-Ring Resonator," *Applied Sciences (Switzerland)*, vol. 12, no. 4, Feb. 2022, doi: 10.3390/app12042144.

[30] C. G. Juan *et al.*, "Feasibility study of portable microwave microstrip open-loop resonator for non-invasive blood glucose level sensing: proof of concept," *Medical & Biological Engineering & Computing*, vol. 57, no. 11, pp. 2389–2405, Nov. 2019, doi: 10.1007/s11517-019-02030-w.

[31] S. Kiani, P. Rezaei, M. Karami, and R. A. Sadeghzadeh, "Band-stop filter sensor based on SIW cavity for the non-invasive measuring of blood glucose," *IET Wireless Sensor Systems*, vol. 9, no. 1, pp. 1–5, Feb. 2019, doi: 10.1049/iet-wss.2018.5044.

[32] V. Turgul and I. Kale, "A novel pressure sensing circuit for non-invasive RF/microwave blood glucose sensors," in *2016 16th Mediterranean Microwave Symposium (MMS)*, Nov. 2016, pp. 1–4. doi: 10.1109/MMS.2016.7803818.

[33] K. Qin, Y. He, Y. Pei, X. Cai, and Y. Luo, "A Microwave Biosensor for Non-invasive Blood Glucose Detection with Accuracy Enhancement," in *2019 International Applied Computational Electromagnetics Society Symposium - China (ACES)*, Aug. 2019, pp. 1–2. doi: 10.23919/ACES48530.2019.9060614.

[34] R. Baghbani, M. A. Rad, and A. Pourziad, "Microwave sensor for non-invasive glucose measurements design and implementation of a novel linear," *IET Wireless Sensor Systems*, vol. 5, no. 2, pp. 51–57, Apr. 2015, doi: 10.1049/iet-wss.2013.0099.

[35] B. R. Jean, E. C. Green, and M. J. McClung, "A microwave frequency sensor for non-invasive blood-glucose measurement," in *2008 IEEE Sensors Applications Symposium*, Feb. 2008, pp. 4–7. doi: 10.1109/SAS.2008.4472932.

[36] V. Turgul and I. Kale, "Influence of fingerprints and finger positioning on accuracy of RF blood glucose measurement from fingertips," *Electronics Letters*, vol. 53, no. 4, pp. 218–220, Feb. 2017, doi: 10.1049/el.2016.4327.

[37] V. Turgul and I. Kale, "Simulating the Effects of Skin Thickness and Fingerprints to Highlight Problems With Non-Invasive RF Blood Glucose Sensing From Fingertips," *IEEE Sensors Journal*, vol. 17, no. 22, pp. 7553–7560, Nov. 2017, doi: 10.1109/JSEN.2017.2757083.

[38] M. N. Hasan, S. Tamanna, P. Singh, M. D. Nadeem, and M. Rudramuni, "Cylindrical Dielectric Resonator Antenna Sensor for Non-Invasive Glucose Sensing Application," in *2019 6th International Conference on Signal Processing and Integrated Networks (SPIN)*, Mar. 2019, pp. 961–964. doi: 10.1109/SPIN.2019.8711633.

[39] S. Pimentel, P. D. Agüero, A. J. Uriz, J. C. Bonadero, M. Liberatori, and J. C. Moreira, "Simulation of a non-invasive glucometer based on a microwave resonator sensor," *Journal of Physics: Conference Series*, vol. 477, p. 012020, Dec. 2013, doi: 10.1088/1742-6596/477/1/012020.

[40] E. Topsakal, T. Karacolak, and E. C. Moreland, "Glucose-dependent dielectric properties of blood plasma," in *2011 XXXth URSI General Assembly and Scientific Symposium*, Aug. 2011, pp. 1–4. doi: 10.1109/URSIGASS.2011.6051324.

[41] M. C. Cebedio, L. A. Rabioglio, I. E. Gelosi, R. A. Ribas, A. J. Uriz, and J. C. Moreira, "Analysis and Design of a Microwave Coplanar Sensor for Non-

Invasive Blood Glucose Measurements," *IEEE Sensors Journal*, vol. 20, no. 18, pp. 10572–10581, Sep. 2020, doi: 10.1109/JSEN.2020.2993182.

[42] M.A. Eleiwa and Atef Elsherbeni, "Debye Constants for Biological Tissues from 30 Hz to 20 GHz," 2001.

[43] S. Seewattanapon, T. Wattakeekamthorn, T. Somwong, and P. Akkaraekthalin, "A microstrip folded resonator sensor for measurement of dielectric constant," in *2008 5th International Conference on Electrical Engineering/Electronics, Computer, Telecommunications and Information Technology*, May 2008, pp. 245–248. doi: 10.1109/ECTICON.2008.4600418.

[44] G. Guarin, M. Hofmann, J. Nehring, R. Weigel, G. Fischer, and D. Kissinger, "Miniature Microwave Biosensors: Noninvasive Applications," *IEEE Microwave Magazine*, vol. 16, no. 4, pp. 71–86, May 2015, doi: 10.1109/MMM.2015.2394024.

[45] B. A. Hovhannisyan, D. S. Hambaryan, L. A. Odabashyan, and A. Zh. Babajanyan, "REAL-TIME SENSING THE GLUCOSE CONCENTRATION BY QUADRATIC-SHAPED MICROWAVE SENSOR," *Proceedings of the YSU A: Physical and Mathematical Sciences*, vol. 53, no. 2 (249), pp. 132–137, Aug. 2019, doi: 10.46991/PYSU:A/2019.53.2.132.

[46] M. Mrozowski and M. A. Stuchly, "Parameterization of media dispersive properties for FDTD," *IEEE Transactions on Antennas and Propagation*, vol. 45, no. 9, pp. 1438–1439, 1997, doi: 10.1109/8.623134.

[47] J. McVay, N. Engheta, and A. Hoorfar, "High impedance metamaterial surfaces using Hilbert-curve inclusions," *IEEE Microwave and Wireless Components Letters*, vol. 14, no. 3, pp. 130–132, Mar. 2004, doi: 10.1109/LMWC.2003.822571.

[48] L. Odabashyan *et al.*, "Real-Time Noninvasive Measurement of Glucose Concentration Using a Modified Hilbert Shaped Microwave Sensor," *Sensors*, vol. 19, no. 24, p. 5525, Dec. 2019, doi: 10.3390/s19245525.

[49] A. E. Omer *et al.*, "Low-cost portable microwave sensor for non-invasive monitoring of blood glucose level: novel design utilizing a four-cell CSRR hexagonal configuration," *Scientific Reports*, vol. 10, no. 1, p. 15200, Dec. 2020, doi: 10.1038/s41598-020-72114-3.

[50] Ahmad H. Abdelgwad, "Microstrip Patch Antenna Enhancement Techniques," *World Academy of Science, Engineering and Technology International Journal of Electronics and Communication Engineering*, vol. 12, no. 10, 2018.

[51] J. Vrba and D. Vrba, "A Microwave Metamaterial Inspired Sensor for Non-Invasive Blood Glucose Monitoring," *Radioengineering*, vol. 24, no. 4, pp. 877–884, Sep. 2015, doi: 10.13164/re.2015.0877.

[52] A. Y. Ardiansyah and R. Sarno, "Performance analysis of wireless sensor network with load balancing for data transmission using xbee zb module," *Indonesian Journal of Electrical Engineering and Computer Science*, vol. 18, no. 1, p. 88, Apr. 2020, doi: 10.11591/ijeecs.v18.i1.pp88-100.

Appendices

Appendix A

Arduino

```
#include <XBee.h>

#include <SoftwareSerial.h>

#include <LiquidCrystal.h>

LiquidCrystal lcd(12,11,5,4,3,2);

// XBee's DOUT (TX) is connected to pin 8 (Arduino's Software RX)

// XBee's DIN (RX) is connected to pin 9 (Arduino's Software TX)

SoftwareSerial serial1(8, 9); // RX, TX

XBee xbee=XBee();

XBeeResponse response = XBeeResponse();

Rx16Response rx16 = Rx16Response();

Rx64Response rx64 = Rx64Response();

uint8_t option = 0;

uint8_t data = 0;

uint8_t rssi = 0;

void setup() {

  Serial.begin(9600);
```

```
    serial1.begin(9600);

  xbee.setSerial(serial1);

  lcd.begin(16,2);

  lcd.clear();}

void loop() {

  xbee.readPacket(100);

  if (xbee.getResponse().isAvailable()) {

   Serial.println("available");

   if(xbee.getResponse().getApiId()        ==        RX_64_RESPONSE        ||
xbee.getResponse().getApiId() == RX_16_RESPONSE)    {

     Serial.println("16");

     if (xbee.getResponse().getApiId() == RX_16_RESPONSE)      {

      Serial.println("16");

      xbee.getResponse().getRx16Response(rx16);

      //option = rx16.getOption();

      //data = rx16.getData(0);

      rssi = rx16.getRssi();

      //Serial.print("data: ");Serial.println(data);

      //Serial.print("option: ");Serial.println(option);

      lcd.clear();

      lcd.print(rssi);

      Serial.println(rssi);     }
```

```
else      {

  Serial.println("64");

  xbee.getResponse().getRx64Response(rx64);

  //option = rx64.getOption();

  //data = rx64.getData(0);

  rssi = rx64.getRssi();

  lcd.clear();

  lcd.print(rssi);

  Serial.println(rssi);      }    }  }}
```

Appendix B

Real-time BGL Estimation via RSSI

```
# libraries

import tkinter as tk

from tkinter import ttk

from tkinter import messagebox

from matplotlib.backends.backend_tkagg import FigureCanvasTkAgg

import matplotlib.pyplot as plt

import numpy as np

import pandas as pd

from matplotlib.figure import Figure

from matplotlib.backends.backend_tkagg import FigureCanvasTkAgg

from sklearn.metrics import r2_score

from sklearn.metrics import mean_squared_error

from sklearn.metrics import mean_absolute_error

from datetime import datetime

import time

import serial
```

```python
import time

import csv

import matplotlib

matplotlib.use("tkAgg")

import matplotlib.pyplot as plt

import numpy as np

# Importing the dataset

dataset = pd.read_csv('C:\Users\mutah\Desktop\MAKALE\datas.csv')

x = dataset.iloc[:, :2].values

y = dataset.iloc[:, 2].values

# Feature Scaling

xtrain, xtest, ytrain, ytest = train_test_split(

    x, y, test_size=0.5, random_state=1)

#Fitting the Support Vector Regression Model to the dataset

from sklearn.preprocessing import StandardScaler

sc_x = StandardScaler()

sc_y = StandardScaler()

sc_X = StandardScaler()

sc_Y = StandardScaler()

x = sc_x.fit_transform(xtrain)

y = sc_y.fit_transform(ytrain.reshape(-1, 1))
```

```python
X=sc_X.fit_transform(xtest)

Y=sc_Y.fit_transform(ytest.reshape(-1, 1))

#Create your support vector regressor

from sklearn.svm import SVR

regressor = SVR()

import time

start_svr = time.time()

regressor.fit(x,y.ravel())

stop_svr = time.time()

#Predicting results

Y_pred = regressor.predict(X)

print("SVR R2 :", r2_score(Y,Y_pred))

print('MSE:',mean_squared_error(Y,Y_pred))

print('MAE:', mean_absolute_error(Y,Y_pred))

print('RMSE:', np.sqrt(mean_squared_error(Y,Y_pred)))

execution_time_svr = stop_svr-start_svr

print('Execution time :', execution_time_svr)

# Decision Tree Regression

# r_dt = DecisionTreeRegressor(min_samples_split=45,min_samples_leaf=7)

# start_dt = time.time()

# r_dt.fit(xtrain, ytrain)
```

```
# stop_dt = time.time()

# y_pred_dt = r_dt.predict(xtest)

# print("Decision Tree R2:", r2_score(ytest, y_pred_dt))

# print('MSE:', mean_squared_error(ytest, y_pred_dt))

# print('MAE:', mean_absolute_error(ytest, y_pred_dt))

# print('RMSE:', np.sqrt(mean_squared_error(ytest, y_pred_dt)))

# execution_time_dt = stop_dt-start_dt

# print('Execution time :', execution_time_dt)

# #Polynomial regression

# from sklearn.linear_model import LinearRegression

# from sklearn.preprocessing import PolynomialFeatures

# poly_reg = PolynomialFeatures(degree=3)

# x_poly = poly_reg.fit_transform(xtrain)

# lin_reg = LinearRegression()

# start_pr = time.time()

# lin_reg.fit(x_poly,ytrain)

# stop_pr = time.time()

# y_pred_lr=lin_reg.predict(poly_reg.fit_transform(xtest))

# #R2 degerleri

# print("Polynomial R2:", r2_score(ytest,y_pred_lr))

# print('MSE:',mean_squared_error(ytest,y_pred_lr))
```

```python
# print('MAE:', mean_absolute_error(ytest, y_pred_lr))

# print('RMSE:', np.sqrt(mean_squared_error(ytest,y_pred_lr)))

# execution_time_pr = stop_pr-start_pr

# print('Execution time :', execution_time_pr)

# import pickle

# pickle.dump(lin_reg ,open("kayıt","wb"))

# yuklenen = pickle.load(open("kayıt","rb"))

# a=yuklenen.predict(poly_reg.fit_transform(xtest))

# print(a)

# ##Random Forest Regresyonu

# from sklearn.ensemble import RandomForestRegressor

# rf_reg = RandomForestRegressor(n_estimators = 100)

# start_rf = time.time()

# rf_reg.fit(xtrain,ytrain)

# stop_rf = time.time()

# y_pred_rf=rf_reg.predict(xtest)

# #R2 degerleri

# print("Random Forest R2:", r2_score(ytest,y_pred_rf))

# print('MSE:',mean_squared_error(ytest,y_pred_rf))

# print('MAE:', mean_absolute_error(ytest, y_pred_rf))

# print('RMSE:', np.sqrt(mean_squared_error(ytest,y_pred_rf)))
```

```python
# execution_time_rf = stop_rf-start_rf

# print('Execution time :', execution_time_rf)

# #Ensemble methods

# from sklearn import ensemble

# from sklearn.ensemble import BaggingRegressor

# bg = BaggingRegressor(DecisionTreeRegressor(), max_samples= 0.6,

#                       max_features = 1.0, n_estimators = 500)

# start_bg = time.time()

# bg.fit(xtrain,ytrain)

# stop_bg = time.time()

# y_pred_bg=bg.predict(xtest)

# print("Bagging R2:", r2_score(ytest,y_pred_bg))

# print('MSE:',mean_squared_error(ytest,y_pred_bg))

# print('MAE:', mean_absolute_error(ytest, y_pred_bg))

# print('RMSE:', np.sqrt(mean_squared_error(ytest,y_pred_bg)))

# execution_time_bg = stop_bg-start_bg

# print('Execution time :', execution_time_bg)

# from sklearn.ensemble import AdaBoostRegressor

# ada    =    AdaBoostRegressor(base_estimator=    DecisionTreeRegressor(),
n_estimators=500)

# start_ada = time.time()

# ada.fit(xtrain,ytrain)
```

```python
# ada.fit(xtrain,ytrain)
```

```python
# stop_ada = time.time()

# y_pred_ada=ada.predict(xtest)

# print("Ada Boost R2:", r2_score(ytest,y_pred_ada))

# print('MSE:',mean_squared_error(ytest,y_pred_ada))

# print('MAE:', mean_absolute_error(ytest, y_pred_ada))

# print('RMSE:', np.sqrt(mean_squared_error(ytest,y_pred_ada)))

# execution_time_ada = stop_ada-start_ada

# print('Execution time :', execution_time_ada)

# from xgboost import XGBRegressor

# xgbr=xgb.XGBRegressor()

# start_xgb = time.time()

# xgbr.fit(xtrain, ytrain)

# stop_xgb = time.time()

# xgbr.score(xtest,ytest)

# y_pred_xgbr=xgbr.predict(xtest)

# print("XgBoost R2:", r2_score(ytest,y_pred_xgbr))

# print('MSE:',mean_squared_error(ytest,y_pred_xgbr))

# print('MAE:', mean_absolute_error(ytest, y_pred_xgbr))

# print('RMSE:', np.sqrt(mean_squared_error(ytest,y_pred_xgbr)))

# execution_time_xgb = stop_xgb-start_xgb

# print('Execution time :', execution_time_xgb)
```

```python
# from lightgbm import LGBMRegressor

# lgbm= lgb.LGBMRegressor()

# start_lgbm = time.time()

# lgbm.fit(x,y.ravel())

# stop_lgbm = time.time()

# y_pred_lgbm=lgbm.predict(X)

# print("LGB R2:", r2_score(Y, y_pred_lgbm))

# print('MSE:',mean_squared_error(Y, y_pred_lgbm))

# print('MAE:', mean_absolute_error(Y, y_pred_lgbm))

# print('RMSE:', np.sqrt(mean_squared_error(Y, y_pred_lgbm)))

# execution_time_lgbm = stop_lgbm-start_lgbm

# print('Execution time :', execution_time_lgbm)

from sklearn.ensemble import GradientBoostingRegressor

params = {'n_estimators': 100, 'max_depth': 4, 'min_samples_split': 2,

        'loss': 'ls','learning_rate':0.6}

gbm = GradientBoostingRegressor(**params)

start_gbm = time.time()

gbm.fit(x,y.ravel())

stop_gbm = time.time()

print("GBM R2:", r2_score(Y, gbm.predict(X)))
```

```python
print('MSE:', mean_squared_error(Y,gbm.predict(X)))

print('MAE:', mean_absolute_error(Y, gbm.predict(X)))

print('RMSE:', np.sqrt(mean_squared_error(Y,gbm.predict(X))))

execution_time_gbm = stop_gbm-start_gbm

print('Execution time :', execution_time_gbm)

# from catboost import CatBoostRegressor

# cbr=CatBoostRegressor(iterations=200,

#                 learning_rate=0.6,

#                 depth=5,

#                 eval_metric='R2',

#                 random_seed = 40,

#                 metric_period = 100)

# start_cbr = time.time()

# cbr.fit(x,y.ravel())

# stop_cbr = time.time()

# print("CBR R2:", r2_score(Y, cbr.predict(X)))

# print('MSE:', mean_squared_error(Y, cbr.predict(X)))

# print('MAE:', mean_absolute_error(Y, cbr.predict(X)))

# print('RMSE:', np.sqrt(mean_squared_error(Y,cbr.predict(X))))

# execution_time_cbr = stop_cbr-start_cbr

# print('Execution time :', execution_time_cbr)import pickle
```

```python
pickle.dump(lin_reg ,open("kayıt","wb"))

yuklenen = pickle.load(open("kayıt","rb"))

# XBee

import serial

ser = serial.Serial('COM4')

ser.flushInput()

while True:

    try:

        ser_bytes = ser.readline()

        decoded_bytes = float(ser_bytes[0:len(ser_bytes)-2].decode("utf-8"))

        # print(decoded_bytes)

        time.sleep(1)

        sp = decoded_bytes  #serial porttan gelecek olan data

        rss = np.array([sp,]).reshape(-1, 1)

        g_conc = int(yuklenen.predict(poly_reg.fit_transform(rss)))

        print(g_conc)

    except:

        print("Keyboard Interrupt")

        break
```

Appendix C

Publications from the Thesis

Conference Papers

1. Kuran M., Palandöken M. Compact Rf Sensing Unit Design for Lte Band Non-Invasive Glucose Sensor Applications, 1. Internatıonal Marmara Scıentıfıc Research And Innovatıon Congress, 2021.

Projects

1. Kan Şekeri Seviyesinin İnvazif Olmayan Şekilde İzlenmesi için Taşınabilir Mikrodalga Sensörü (2021-TYL-FEBE-0014, İKÇÜ-MERLAB Supported Project)

Curriculum Vitae

Name Surname   : Mutahhar KURAN

E-mail (1)   : Y190207007@ogr.ikcu.edu.tr

E-mail (2)   : mutaharakuran@hotmail.com

Education:

2014–2019   İzmir Kâtip Çelebi University, Dept. of Electrical-Electronics Eng.

2019–2022   İzmir Kâtip Çelebi University, Dept. of Electrical-Electronics Eng.

Work Experience:

2019 – 2020   TUBITAK Project Researcher fellow

2019 – Now   Freelancer.com, Freelancer

2021 – Now   R&D Engineer, Aren5 Simülasyon Teknoloji Yatırım A.Ş.

Publications:

1. Power Lines Magnetic Field Energy Harvesting Device

M Kuran, M Palandöken - International Black Sea Coastline Countries Symposium-II, 2019

2. Compact Rf Sensing Unit Design For Lte Band Non-Invasive Glucose Sensor Applications

M Kuran, M Palandöken - 1. Internatıonal Marmara Scıentıfıc Research And Innovatıon Congress -II, 2021